https://dx.doi.org/10.21577/0103-5053.20220104

J. Braz. Chem. Soc., Vol. 34, No. 2, 242-262, 2022
©2022 Sociedade Brasileira de Química

Article

Theoretical and Experimental Spectroscopic Study on 2-Chloro-3-(substituted-phenylamino)-1,4-naphthoquinone Derivatives

Flaviana R. F. Dias,[a] Vinícius R. Campos,[a] Raphael S. M. de Moraes,[a] Nelson A. Souza,[a] Anna C. Cunha,[a] Mateus R. Lage[b] and Glaucio B. Ferreira,[c]*

[a]*Departamento de Química Orgânica, Instituto de Química, Universidade Federal Fluminense, Campus do Valonguinho, 24020-141 Niterói-RJ, Brazil*

[b]*Universidade Federal do Maranhão, Campus Balsas, Rua José Leão, 484, Centro, 65800-000 Balsas-MA, Brazil*

[c]*Departamento de Química Inorgânica, Instituto de Química, Universidade Federal Fluminense, 21945-970 Rio de Janeiro-RJ, Brazil*

The 1,4-naphthoquinones are an important group of compounds intensively studied because of their wide range of biological activities. Four 2-chloro-3-(substituted-phenylamino)-1,4-naphthoquinone derivatives were synthesized, and the vibrational modes of these molecules were assigned using Raman and Fourier transform infrared spectroscopy (FTIR) techniques. In addition, X-ray studies were performed for one of these derivatives. Density functional theory (DFT) calculations were also developed for these compounds and presented. In summary, the results obtained from these studies can assess chemical changes in the structures of functionalized quinones and the discovery of candidate biologically active compounds.

Keywords: 1,4-naphthoquinones, Raman spectroscopy, FTIR, DFT

Introduction

Quinones represent a privileged class of biologically active[1-6] that play an important role in biological electron transfer processes (e.g., photosynthesis and respiration)[7,8] and a variety of industrial applications in color chemistry such as hair dyeing, photosensitizers, and anion sensors.[9-12]

In the field of chemotherapy, several quinone derivatives, such as anthracyclines, are clinically important drugs used in cancer treatment.[13] In particular, aminoquinone frameworks show different activities, acting as antitumoral, antimicrobial, antimalarial, antifungal and molluscicidal.[14-18]

Quinones exert their biological effects via quinone-hydroquinone redox cycling, leading to reactive oxygen species (ROS) generation, such as superoxide anion radical ($O_2^{\bullet-}$) and hydroxyl radical (•OH).[19] ROS production leads to an oxidant-antioxidant imbalance or oxidative stress and can lead to irreversible biomolecules damage such as lipids, proteins, ribonucleic acid (RNA), and deoxyribonucleic acid (DNA), followed by cell death.[20,21] Other DNA damage mechanisms associated with quinone derivatives include DNA alkylating reaction and intercalation in the DNA double helix.[22]

The quinone redox cycle may be influenced by adding electron-attracting or donating substituents to the quinoid system. In this context, quinone compounds containing a substituted amino group in their structures have been identified by our research group as having biological activities against different targets.[3-5] Aminoquinone derivatives have also been used as a potential building block for the synthesis of bioactive modified quinones.[14,15,19]

Several computational and structural X-ray diffraction studies,[18,23-25] in search for quantitative three-dimensional correlation structure-property (3D-QSAR)[26] have aided in the comprehension of these biological applications. The evaluation of the importance of intramolecular electronic properties, such as parameters highest occupied molecular orbital (HOMO) and lowest unoccupied molecular orbital (LUMO) energies, hardness, atomic charges, dipole moment, polarizability, molecular volume and Gibbs free energy, can provide indications of potential target molecules. Moreover, the crystalline package containing intermolecular interactions of the classic

*e-mail: glauciobf@gmail.com
Editor handled this article: Brenno A. D. Neto (Associate)

and non-classical hydrogen bond type can justify the importance of the biophoric sites of these substances.[27] However, theoretical-experimental studies of vibrational and electronic spectroscopy containing a quinonoidic ring have placed great emphasis on *p*-benzoquinone and its derivatives,[28,29] with a reduced approach to studies of complete aminoquinone assignment. Such techniques are routinely used in the quality control of pharmaceutics and may allow the identification and distinction of crystal forms.[30,31]

In this work, we described the synthesis, evaluated a new crystal structure, and investigated how electron-donating substituents by inductive effect and by resonance effect affect the electronic structure, molecular topology and vibrational properties of 2-chloro-3-(substituted-phenylamino)-1,4-naphthoquinone derivatives (Figure 1).

Experimental

All reagents and solvents used in the preparation of substances **1a-1d** were used without purification. The progress of the reactions was routinely monitored by thin layer chromatography (TLC) on silica gel plates (60F-F254) aluminum sheets 20 × 20 cm (Merck KGaA, Darmstadt, Germany) and visualized using ultraviolet light (UV-254 and 366 nm). The eluent mixture used was prepared volume by volume (v/v). Compounds **1a-1d** had their respective melting points (mp) determined with a Fisher Johns instrument (Niterói, Brazil), which are uncorrected. Purification of compounds was carried out by silica gel flash column chromatography from Merck (Darmstadt, Germany). Hydrogen nuclear magnetic resonance spectra (^{1}H NMR) were performed using $CDCl_3$ as solvent (Sigma-Aldrich, São Paulo, Brazil) using a Varian Unity Plus 500 MHz spectrometer and tetramethylsilane (TMS) as an internal standard. The respective chemical shifts (δ) were expressed in parts *per* million (ppm) and the coupling constant (J) in hertz.

Synthesis of 2-chloro-3-(phenylamino)-1,4-naphthoquinone derivatives **1a-1d**

The synthesis of 2-chloro-3-(substituted-phenylamino)-1,4-naphthoquinone derivatives **1a-1d** (Figure 2) was achieved by nucleophilic substitution between anilines **3a-3d** and 2,3-dichloro-1,4-naphthoquinone (**2**) with high yield when anilines substituted with electron donating groups are used. Thus, following these principles, the preparation and characterization of the compounds **1a-1d** are described below.

In a 50 mL flask bottom, 0.5 mmol of 2,3-dichloro-naphthoquinone (**2**) in 10 mL of water and 0.5 mmol of aniline **3a** or the analogues substituted **3b-3d** were added. The mixture was kept under stirring at room temperature for 20 h. Upon completion of the reaction, they were filtered through a vacuum, and the precipitate was washed with water. Then, the substituted 2-amino-1,4-naphthoquinones **1a-1d** were purified by chromatography column on a silica gel using a blend of hexane/ethyl acetate (7:3) as eluent. The solid obtained had a yield ranging from 84 to 90%.[21]

2-Chloro-3-(phenylamino)-1,4-naphthoquinone (**1a**)

The substance **1a** was obtained as a burgundy solid; mp 214-216 °C, in 85% yield; IR (film) ν_{max} / cm^{-1} 3232, 1674, 1634, 1561; ^{1}H NMR (500.00 MHz, $CDCl_3$) δ 7.08 (d, 2H, J 7.5 Hz, H-2'/H-6'), 7.22 (t, 1H, J 7.5 Hz, H-4'), 7.35 (dd, 2H, J 7.5, 2.5 Hz, H-3'/H-5'), 7.68 (s, 1H, N-H), 7.70 (td, 1H, J 7.5, 1.5 Hz, H-6), 7.77 (td, 1H, J 9.0, 1.0 Hz,

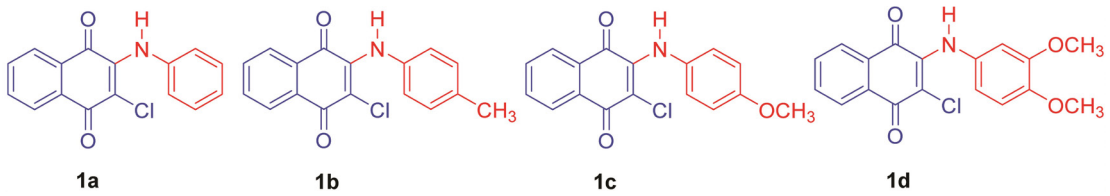

Figure 1. Structure of 2-chloro-3-phenylamino-1,4-napthoquinone (**1a**), 2-chloro-3-((4-methylphenyl)amino) (**1b**), 2-chloro-3-((4-methoxyphenyl)amino)-1,4-napthoquinone (**1c**), and 2-chloro-3-((3,4-dimethoxyphenyl)amino)-1,4-napthoquinone (**1d**).

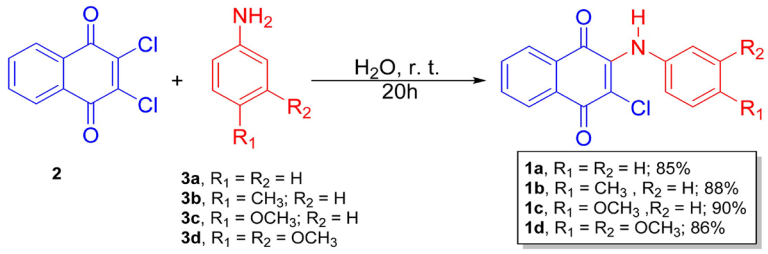

Figure 2. Reaction scheme of 2-chloro-3-(phenylamino)-1,4-naphthoquinone derivatives.

H-7), 8.12 (dd, 1H, *J* 7.5, 1.0 Hz, H-5), 8.19 (dd, 1H, *J* 8.0, 1.0 Hz, H-8).

2-Chloro-3-(4-methylphenylamino)-1,4-naphthoquinone (**1b**)

The substance **1b** was obtained as a burgundy solid; mp 184-186 °C, in 88% yield; IR (film) ν_{max} / cm^{-1} 3220, 1674, 1636, 1563; ^{1}H NMR (500.00 MHz, $CDCl_3$) δ 2.37 (s, 3H, C$\underline{H}_3$), 7.01 (d, 2H, *J* 8.0 Hz, H-2'/H-6'), 7.15 (d, 2H, *J* 8.5 Hz, H-3'/H-5'), 7.68 (td, 1H, *J* 7.5, 1.0 Hz, H-6), 7.76 (td, 1H, *J* 7.5, 1.5 Hz, H-7), 8.11 (dd, 1H, *J* 7.5, 1.0 Hz, H-5), 8.19 (dd, 1H, *J* 7.5, 1.0 Hz, H-8).

2-Chloro-3-(4-methoxyphenylamino)-1,4-naphthoquinone (**1c**)

The substance **1c** was obtained as a burgundy solid; mp 221-223 °C, with 90% yield; IR (film) ν_{max} / cm^{-1} 3247, 1674, 1636, 1565; ^{1}H NMR (500.00 MHz, $CDCl_3$) δ 3.83 (s, 3H, OC$\underline{H}_3$), 6.88 (dd, 2H, *J* 6.5, 2.0 Hz, H-2'/H-6'), 7.05 (dd, 2H, *J* 7.0, 2.0 Hz, H-3'/H-5'), 7.63 (s, 1H, N-H), 7.67 (td, 1H, *J* 7.5, 1.0 Hz, H-6), 7.76 (td, 1H, *J* 7.5, 1.0 Hz, H-7), 8.11 (dd, 1H, *J* 8.0, 1.0 Hz, H-5), 8.18 (dd, 1H, *J* 8.5, 1.0 Hz, H-8).

2-Chloro-3-(3,4-dimethoxyphenylamino)-1,4-naphthoquinone (**1d**)

The substance **1d** was obtained as a burgundy solid, with 86% yield; mp < 300 °C; IR (film) ν_{max} / cm^{-1} 3222, 1670, 1636, 1563; ^{1}H NMR (500.00 MHz, $CDCl_3$) δ 3.87 (s, 3H, OC$\underline{H}_3$), 3.90 (s, 3H, OC$\underline{H}_3$), 6.66 (d, 1H, *J* 2.5 Hz, H-2'), 6.69 (dd, 1H, *J* 8.5, 2.5 Hz, H-6'), 6.82 (d, 2H, *J* 2.5 Hz, H-5'), 7.66 (s, 1H, N-H), 7.69 (td, 1H, *J* 7.5, 1.0 Hz, H-6), 7.77 (td, 1H, *J* 7.5, 1.0 Hz, H-7), 8.11 (dd, 1H, *J* 7.5, 1.0 Hz, H-5), 8.19 (dd, 1H, *J* 8.0, 1.0 Hz, H-8).

Single crystal X-ray

Single crystal X-ray data for **1d** were collected on a Bruker D8 Venture diffractometer (Niterói, Brazil) using graphite-monochromated Mo Kα radiation (λ = 0.71073 Å) at 298 K. Data collection, cell refinement and data reduction were performed with Bruker Instrument Service v4.2.2, APEX3 and SAINT,[32,33] respectively. The absorption correction using equivalent reflections was performed with the SADABS program.[34] The structure solutions and full-matrix least-squares refinements based on F^2 were performed with the SHELX package.[35,36] All H atoms were refined with fixed individual displacement parameters [Uiso\(H) = 1.2 Ueq (Csp^2 and C_{ar}) or 1.5 U_{eq} (Csp^3)] using a riding model. All non-hydrogen atoms were refined anisotropically. Structure illustrations were generated using ORTEP-3 for Mercury and the crystallographic tables were constructed using Olex2.[37,38]

The equipment is located at the Multiuser X-Ray Diffraction Laboratory, LDRX-UFF of the Instituto de Física of the Universidade Federal Fluminense, Brazil.

Vibrational and electronic spectroscopy

The Fourier transform infrared (FTIR) spectra were measured on Nicolet™ iS50 (Niterói, Brazil) spectrometer equipment with an attenuated total reflectance accessory and LaTGS detector for the ranges of 4000-400 cm^{-1} and 600-50 cm^{-1} with an average of 128 scans at room temperature with 4 cm^{-1} resolution. Data analysis was performed on the Omnic software.

The FT-Raman spectra were obtained using a Bruker MultiRAM spectrometer (Niterói, Brazil) in the region between 3500-70 cm^{-1} with 2 cm^{-1} resolution. The exciting laser wavelength radiation (Nd:YAG laser line as the excitation source) presented a wavelength of 1064 nm, and the spectra were recorded at room temperature with a germanium detector kept in liquid nitrogen. The samples were measured in the hemispheric opening of an aluminum sample holder. Data analysis was performed using the OPUS software.

The UV-visible measurements were done in the solid state diluted in MgO and in an acetonitrile solution using a Cary 5000, UV-Vis NIR spectrometer (Niterói, Brazil) and a Cary 50, UV-Vis spectrometer (Niterói, Brazil), respectively. Both measurements were performed from 190 to 800 nm with 0.1 s nm^{-1} resolution. Data analysis was performed using the Cary WinUV software.

The equipment are located at the Multiuser Spectroscopy Laboratory (LAME-UFF) of the Instituto de Química of the Universidade Federal Fluminense, Brazil.

Calculations

The molecular properties were evaluated using the program Gaussian 09 for Linux,[39] with the CAM-B3LYP functional for the development of the density functional theory (DFT) calculation. This functional was selected because it describes the high accuracy systems, including corrections for a better description of long-range interactions.[40,41] A theoretical polar environment was simulated by means of the integral equation formalism in the implicit solvation method of the polarizable continuous model (IEFPCM) implicit solvation method,[42] using acetonitrile, dichloromethane and dimethyl sulfoxide (DMSO) as solvents to emulate possible intermolecular interactions around the analyzed molecules. The basis

set used for developing of all the calculations was the double zeta 6-311G(d,p) for all atoms.[43] The partial atomic charges and the electrostatic potential surfaces (ESP) were calculated according to the Merz-Singh-Kollman scheme.[44,45] The evaluation of the molecular orbitals was carried out using a Mulliken population analysis, and the percentage of atomic orbitals and the graphical population analysis software GaussSum were employed.[46] Every visualization and check of the calculated data were done through the ChemCraft 1.8 program.[47]

Using as a starting point different conformations for the molecular units containing different dihedral angles between the quinone and the phenyl group, interconnected by the amino group, the most stable structural variations of the molecular units of the compounds were analyzed together with their vibrational spectra for acetonitrile data without the presence of imaginary harmonic vibrational modes, indicating that the analysis of isolated units alone, such as neglecting the intermolecular interactions, still allowed good agreement between the calculated and experimental data (crystallographic). The vibrational wavenumber, Raman scattering, and infrared adsorption intensities were visualized through the potential energy distribution (PED) analysis using the VEDA 4 software.[48] The natural bond orbital (NBO) analysis was performed to calculate the natural charge, and analyze a donor-acceptor energy and the natural resonance theory (NRT) provides the analysis of the molecular electron density in terms of resonance structures and weights.[49-53]

Transition energies and oscillator strengths in the UV-Vis spectra of the optimized structures were obtained from time-dependent density functional theory (TD-DFT) calculations. The evaluation of the theoretical methods was accomplished using the first 50 lowest energy states in the solution. The analysis of the TD-CAM-B3LYP states and the spectra simulation were carried out with the GaussSum software, using Gaussian functions with half-widths of 3000 cm^{-1}.[46]

The cluster computers and programs used are located at the Multiuser Computational Chemistry Laboratory, LMQC-UFF, of the Instituto de Química of the Universidade Federal Fluminense, Brazil.

Results and Discussion

Structures

Structural analysis of compounds listed in this study, such as **1a** and **1b**, are reported in the literature.[54,55] The main characteristic confirmed is that the phenyl and naphthoquinone rings are not in the same plane. The compounds **1a** and **1b** present crystalline packing with P21/c and Pna21 group spaces, respectively. This class of compounds present intermolecular interaction, with detached for hydrogen bonds connected by systems with N…O in the range from 2.70 to 3.05 Å, which can be treated as resonance assisted hydrogen bonding. Thus, NH…O(2) interaction in **1a** and **1b** is observed between adjacent units involving the amine and carbonyl group of naphthoquinone which is vicinal to the halogen group.

We also studied the 2-chloro-3-((4-methoxyphenyl) amino)-1,4-naphthoquinone (**1c**) by X-ray diffraction. Red single crystals were successfully grown from ethanol by the slow solvent evaporation method at room temperature. The unit cell parameters of the 2-chloro-3-((4-methoxyphenyl) amino)-1,4-naphthoquinone (**1c**) crystal were obtained from the single crystal X-ray diffraction analysis using a Bruker D8 Venture diffractometer with graphite-monochromated Mo Kα radiation (λ = 0.71073 Å) at 298 K. The calculated lattice parameters were a = 12.12 Å, b = 24.16 Å, c = 4.76 Å, α = 90°, β = 90°, γ = 90°, and volume (V) = 1397.3 $Å^3$. The grown crystal belonged to an orthorhombic crystal system with space group $Pna2_1$. Figure 3 shows the Oak Ridge thermal ellipsoid plot (ORTEP) diagram of the compound. Table S1 of the Supplementary Information (SI) section provides the crystal data and refinements. The resonance assisted hydrogen bonding effect was not as relevant, with an N…O distance of 3.075 Å and NH…O of 131.9º, unlike for other structures.

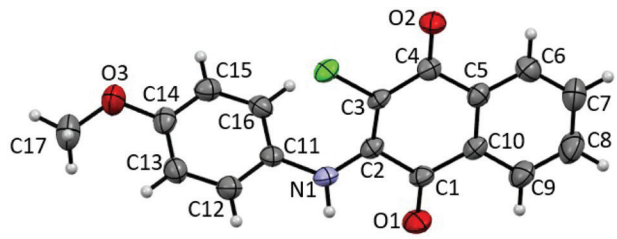

Figure 3. Asymmetric unit representation of 2-chloro-3-((4-methoxy-phenyl)amino)-1,4-naphthoquinone (**1c**) (ellipsoids at 50% probability).

Finally, even though we did not perform an X-ray diffraction structural analysis for the **1d** compound, we evaluated the skeleton centered on the secondary amine between the naphthoquinone and phenyl groups for the 2-chloro-3-((3,5-dimethoxyphenyl)amino)-1,4-naphthoquinone.[56] This compound presents a P-1 space group with the smallest resonance assisted hydrogen bonding effect, presenting an N…O distance of 3.227(3) Å, as observed for the **1c** structure.

The structural properties observed from the optimized geometries obtained from the theoretical study agree with those obtained from the crystallographic study, regardless of considering solvent effects with the integral equation formalism variation of the polarizable continuum model

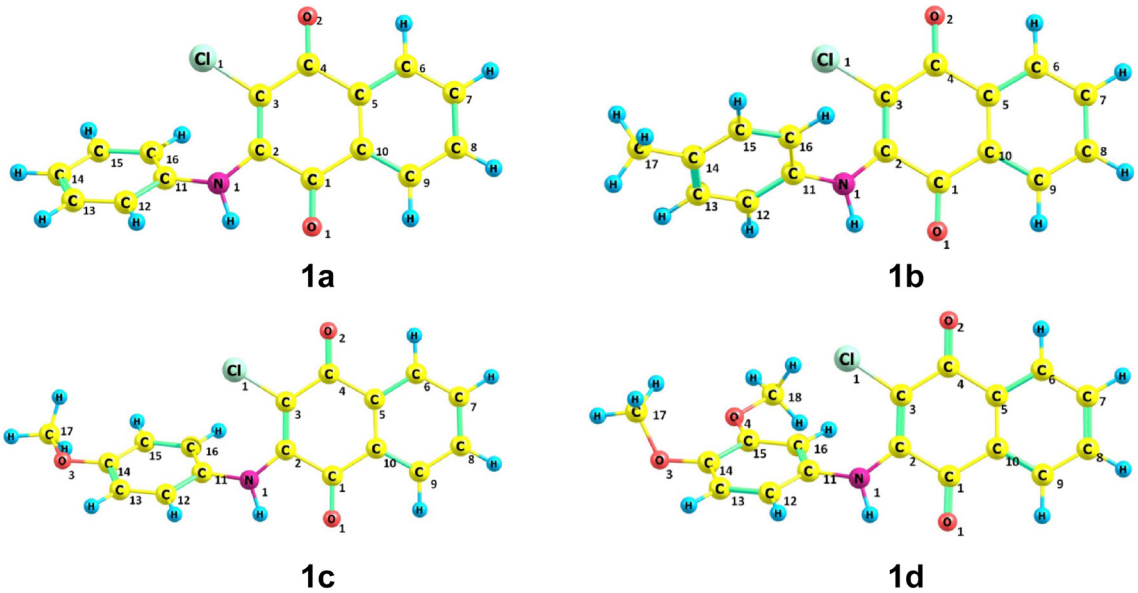

Figure 4. Optimized geometries of the compounds **1a-1d**.

(IEFPCM). As shown in Figure 4, the optimized structural skeleton is centered on the secondary amide group. Theoretical values, such as the $C_{11}N_1C_2$ angle, were close to 130º, and the $C_{11}N_1C_2C_3$ presented dihedral angles ranging from 25 to 30º. The first showed a variation of 2º and the second, with values ranging from 3 to 7º compared to the experimental values.

The observed variations may be related to the crystalline packing, highlighting the identified intermolecular forces, especially for the short distance bonds N–H…O and N–H…Cl.[54-56] The other studied parameters from the theoretical calculations agree with the experimental results, as observed in Table 1 and Tables S2 and S3 found in SI section.

The analysis by root-mean-square deviation (RMSD) was performed to facilitate the comparison of crystallographic data with theoretical data and the results are shown in Figure S1 of the SI section. Note that, in this analysis, only the compounds **1a**, **1b**, and **1c** were evaluated because their molecular structures present higher similarity. The observed results indicate a reasonable approximation between the IEFPCM-optimized data and the crystallographic data, with RMSD < 0.5. The theoretical data resulted in divergence only in the methoxy group in **1c**, with RMSD = 0.40. Therefore,

Table 1. Comparison of calculated (CAM-B3LYP/IEFPCM in MeCN) and experimental (X-ray) geometrical parameters, in compounds **1a-1d**

Geometric parameter / Å	**1a**	X-ray[a]	**1b**	X-ray[b]
$C{=}C_{(Benz.\ and\ Naphtq.)}$	1.361-1.517	1.367-1.508	1.362-1.517	1.374-1.500
$C{=}O_{(Naphtq.)}$	1.212-1.216	1.210-1.227	1.212-1.216	1.218-1.229
$N{-}C_{(Benz.\ and\ Naphtq.)}$	1.349-1.417	1.335-1.410	1.347-1.419	1.345-1.412
$C{-}C_{(-CH3)}$			1.505	1.507
$C{-}Cl_{(Naphtq.)}$	1.738	1.732	1.739	1.727
$C{-}C{-}C_{(Benz.\ and\ CH3)}$			121.02	121.30
$C{-}N{-}C_{(Benz.\ and\ Naphtq.)}$	130.14	128.82	130.07	128.95
$C{-}N{-}C{-}C_{(Benz.\ and\ Naphtq.)}$	29.63	21.34	28.31	25.16
	1c	X-ray[c]	**1d**	X-ray[d]
$C{=}C_{(Benz.\ and\ Naphtq.)}$	1.363-1.518	1.370-1.441	1.361-1.517	1.364-1.502
$C{=}O_{(Naphtq.)}$	1.212-1.217	1.207-1.230	1.212-1.216	1.218-1.223
$N{-}C_{(Benz.\ and\ Naphtq.)}$	1.345-1.421	1.345-1.415	1.348-1.419	1.347-1.419
$C{-}O_{(-OCH3)}$	1.355-1.420	1.372-1.422	1.353-1.429	1.356-1.412
$C{-}Cl_{(Naphtq.)}$	1.741	1.735	1.739	1.717
$C{-}O{-}C_{(Benz.\ and\ CH3)}$	118.42	117.15	115.10-118.37	117.32-118.92
$C{-}N{-}C_{(Benz.\ and\ Naphtq.)}$	130.11	127.69	130.10	128.43
$C{-}N{-}C{-}C_{(Benz.\ and\ Naphtq.)}$	25.18	29.39	28.64	34.79
$C{-}O{-}C{-}C_{(Benz.\ and\ CH3)}$	0.24	1.84	0.87-73.34	3.06-6.52

[a]Reference 54; [b]reference 55; [c]this work; [d]reference 56. Benz.: benzene ring; Naphtq.: naphthoquinone ring.

these results indicate that bond length and bending in the 2-chloro-3-phenylamino-1,4-napthoquinones skeleton are close to those determined experimentally, demonstrating that the theoretical approach can describe the system with great accuracy and contribute to understanding additional topics, such as vibrational and electronic spectra. Even though **1d** has not been analyzed in isolation without considering the crystalline structure, it is clear that it follows the same trend as the other compounds in this study.

Finally, by evaluating the partial atomic charges calculated through the Merz-Singh-Kollman (MSK) and natural charge scheme, as available in Tables S4 and S5 in the SI section, it was possible to identify the influence of the more electronegative atoms that result in the stronger intermolecular interactions. For example, in all molecules **1a**-**1d**, oxygen (O_1 and O_2) and nitrogen (N_1) atoms have the more negative charge values. These atoms are then involved in the main interactions detected in the crystal packing. The amino group has a hydrogen atom with a strong positive charge. It indicates an electron deficiency that justifies the formation of hydrogen bonds. The other oxygen atoms of the methoxy groups through MSK charge for the compounds **1c** and **1d** also have a negative charge, but due to the position of the amino group in the benzene ring, an inductive effect that removes electron density is perceived. This observation was not corroborated by the natural charge obtained by the NBO calculation, since the partial atomic charges of the oxygen atoms show similar values, as observed in Table S5.

Interestingly, even though **1c** has a methoxy group that is an electron density donor by resonance effect in the *para* position, the charge concentration on the nitrogen atom of the amino group is higher than the previous cases in **1d**; however, it is still lower than the compound without a substituent (Figure 5). The evaluation of the charges of the naphthoquinone groups showed certain regularity regardless of the compounds evaluated. The oxygen (O_2) that is adjacent to the chlorine group linked to carbon (C_3) has a charge concentration higher than the oxygen (O_1) adjacent to the amino group.

A recent study by Rajalakshmi *et al.*[54] using several substituents in the phenyl group indicated the effect on the amino group when the nature of the inductive and resonance effects could affect NH group's acidity and the action itself in the hydrogen bonds between adjacent units. For example, the compound 3-chloro-2-(4-chlorophenylamino)-1,4-naphthoquinone presents in its crystalline packaging with an N…O distance of 2.966 Å and NH…O of 131.4º with N–C_{phenyl} of 1.407 Å. In this case, the chloro substituent on the phenyl group has a weak deactivating action. This implies an action of removing the electron density of the amine group, which makes it more acidic. In addition, the quinone ring has an O=C–C=C–NHR π-conjugated system that allows evaluating this effect on the C=O bond distance (1.233 Å), which is longer than the reference molecule **1a** unsubstituted (1.227 Å). Specifically for molecule **1c** of our work, containing a methoxy substituent on the phenyl group, which is a strong activating substituent (Figure 5), an increase in the N(1)–C(11) bond distance to 1.415 Å is observed, according to the X-ray diffraction. This distance was greater than the N–C_{phenyl} distance for compounds **1a** (1.410 Å) and **1b** (1.412 Å) in X-ray diffraction,[54,55] where the first is unsubstituted and the second has a methyl substituent which is a weak activator group. Associated with the C=O bond distance vicinal to the chloro group of quinone, with values of 1.229 and 1.230 Å, respectively for compounds **1b** and **1c**, the effect of resonance assisted hydrogen bonding confirms the influence of the substituents in the phenyl group (R). The crystalline packaging for **1a**, **1b** and **1c** present N…O distance from 3.049 to 2.983 Å.[54]

These crystallographic observations were corroborated by the theoretical data since the RMSD analysis indicated great similarity between the experimental and theoretical structures. But to support this observation, we performed an analysis by natural resonance theory (NRT) that indicates the percentage contribution of

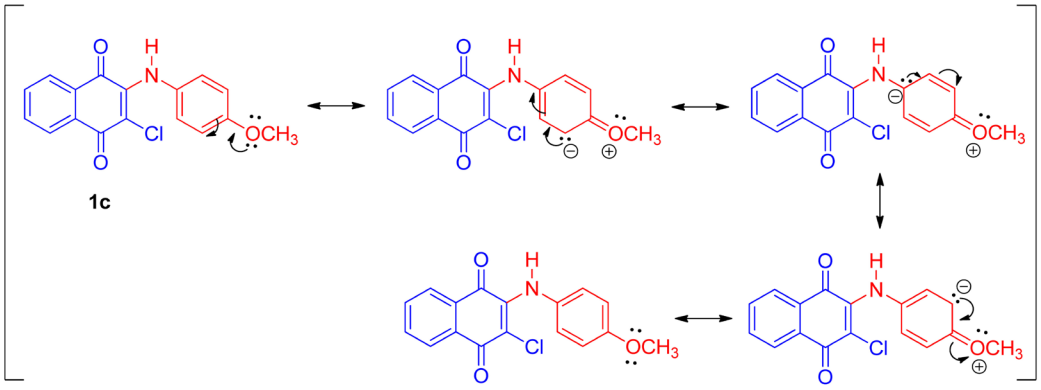

Figure 5. Resonance structures of the compound **1c**.

different resonance structures in relation to a reference and prediction of NBO delocalization, available in Tables S6-S9 in the SI section. The highest weight of structures with a concentration of partial positive atomic charge on the nitrogen atom of the amine was found for the structure of compound **1a** (26.15%), followed by structures of compound **1b** (18.69%) and finally for compounds **1c** and **1d** (6.87 and 6.48%). This indicates the effect of the methoxy substituent with an activating action on the phenyl group, increasing the charge density on the amino group, which makes it more basic.

Figure 6 shows the electrostatic potential surfaces (ESP) of the molecules. These surfaces permit interpreting the overall charge distribution of the molecules. The red color describes the higher concentration of negative charges, while the blue color describes the most positive sites. The hydrogen atom of the amino group is the most positively charged. Contrarily, the oxygen (O) in the carbonyl group of naphthoquinones is the most negatively charged atom, corroborating information described in the literature for these functional groups in naphthoquinone systems.[20] In terms of the electrostatic aspect, the benzenoid ring has a neutral characteristic even in the presence of more electronegative atoms while the naphthoquinone group is positively charged.

Vibrational analyses

Theoretical-experimental vibrational studies involving compounds containing the 1,4-naphtoquinone group have been reported in recent years using density functional theory assistance through the B3LYP hybrid method with different double or triple zeta basis functions with or without pseudopotential, in addition to the use of an implicit solvent method for the study of solvation effects.[57,58] The use of techniques such as potential energy distribution (PED) analysis of theoretical vibrational spectra is also reported. However, as they are the simplest target molecules and have non-functionalized amino groups or only the functionalized 1,4-naphtoquinone molecule, the observed spectra are simpler and have fewer bands and fewer couplings than the molecules in this study.[59,60]

Thus, solid-state experimental spectra for compounds show characteristic bands of the most important chemical groups in each compound between 4000 and 600 cm^{-1} in Figure 7 and from 600 to 150 cm^{-1} in Figure S2 (SI section). The broad band of the amino group in the infrared and Raman spectra and multiple bands between 1675 and 1500 cm^{-1} due to C=C and C=O stretching modes are the most evident bands. The complete assignment of all spectra is given below, with five regions considered: 3500-2800, 1800-1300, 1300-1200, 1000-600 and 600-150 cm^{-1}, where the first four regions belong to the mid-infrared spectrum and the latter to the far-infrared spectrum. This division was also accompanied by the Raman spectrum.

All vibrational modes of the four compounds **1a-1d** were classified as part of either the benzene ring or the naphthoquinone ring. The substituents were identified as methoxy or methyl groups according to the components of each derivative, as illustrated in Figure 7.

The molecules presented between 84 and 96 normal vibrational modes in the theoretical spectra. Tables 2-5 describe the experimental Raman and infrared wavenumbers and the unscaled theoretical values obtained at CAM-B3LYP/6-311G(d,p) level up to 600 cm^{-1}. The

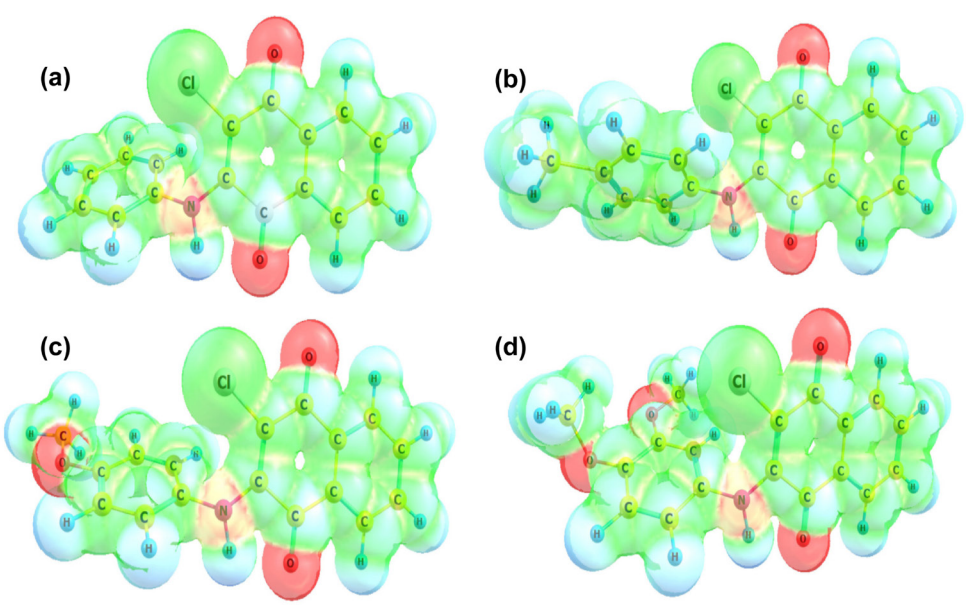

Figure 6. Electrostatic potential surfaces (range: −0.002 to 0.05) of the compounds **1a-1d** in MeCN.

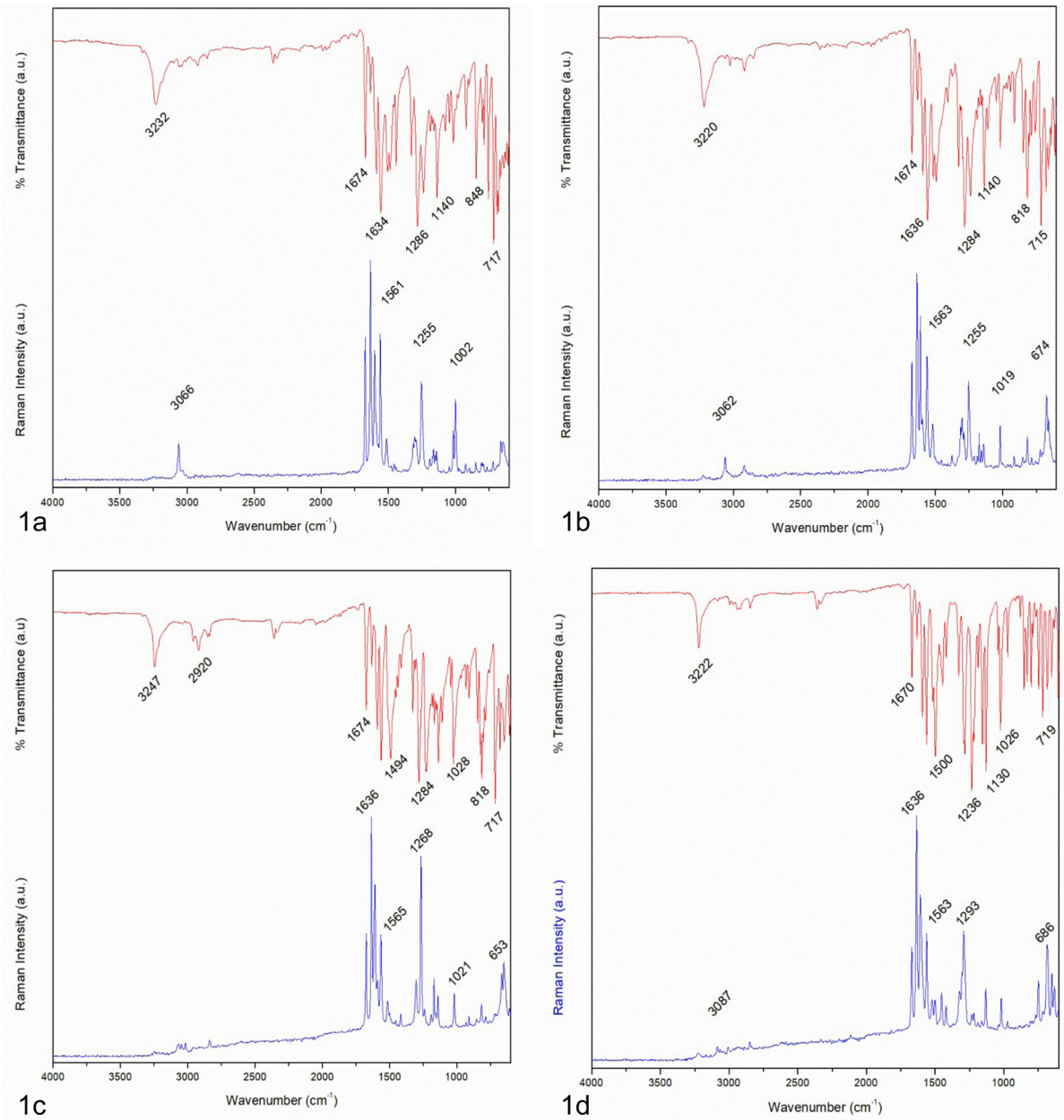

Figure 7. Experimental Raman (blue) and infrared (ATR, red) spectra of the compounds **1a-1d** between 4000-600 cm^{-1}.

complete tables with all the theoretical vibrations are available in the SI section (Tables S10-S13).

Assignment of the normal modes was done using Veda 4.1 software,[48] which performs potential energy distribution analyses to identify the most significant components in each vibrational mode and describes them using internal coordinates. The percentage contributions of each coupled mode at the same frequency were indicated in parentheses. The sum of all possible representations for a given vibrational mode was indicated by the sum of multiple assignments.

The theoretical and experimental wavenumbers showed high correlation for the regions between 3100 and 150 cm^{-1}. The coefficient of determination (R^2) for the correlation between experimental and theoretical wavenumbers was between 0.998 and 0.999. These results are available in the SI section (Figure S3). Thus, by simulating the theoretical spectra according to the values of the calculated scale factors between 0.953 and 0.960, there was a good theoretical and experimental correlation, wherein the intensities of the spectra were comparable and allowed adequate assignment. Scaling factors were applied to the calculated wavenumbers in the SI section (Tables S10-S13).

Discussion of the spectra: region between 4000-2800 cm^{-1}

The region observed at 3350-3150 cm^{-1} in all spectra

Table 2. Experimental and theoretical vibrational wavenumbers of **1a**

Experimental wavenumber / cm^{-1}		Calculated wavenumber / cm^{-1}	IR intensity / cm^{-1}	Raman intensity / cm^{-1}	PED / %
Infrared	Raman				
3234		3539	234.03	1312	$\upsilon_{NH\ Naphtq.}$ (100)
	3066	3222	7.32	1534	$\upsilon_{CH\ Benz.\ Sym.}$ (90)
3062		3216	20.97	245	$\upsilon_{CH\ Benz.\ Asym.}$ (90)
3039	3040	3208	20.85	437	$\upsilon_{CH\ Benz.\ Asym.}$ (86)
1674	1675	1781	338.78	7980	$\upsilon_{C=O\ Naphtq.}$ (85)
1635	1635	1754	318.10	11942	$\upsilon_{C=O\ Naphtq.}$ (81)
1603	1604	1683	101.46	13764	$\upsilon_{CC\ Naphtq.} + \upsilon_{CC\ Benz.}$ (63)
1591		1670	224.70	515	$\upsilon_{CC\ Naphtq.} + \upsilon_{CC\ Benz.}$ (48)
	1577	1666	105.70	204	$\upsilon_{CC\ Benz.}$ (57)
1558	1561	1644	928.64	11886	$\upsilon_{CC\ Naphtq.}$ (51)
1506	1515	1576	837.28	2959	$\upsilon_{CC\ Naphtq.}$ (21); $\delta_{HNC\ Naphtq.}$ (54)
1489	1488	1545	39.82	631	$\rho_{HCCH\ Benz.}$ (50)
	1480	1536	55.73	173	$\rho_{HCCH\ Naphtq.}$ (49); $\delta_{CCC\ Naphtq.}$ (23)
1460	1459	1508	6.47	97	$\upsilon_{CC\ Naphtq.}$ (26); $\rho_{HCCH\ Naphtq.}$ (51)
1442	1446	1499	72.85	292	$\upsilon_{CC\ Benz.}$ (23); $\rho_{HCCH\ Benz.}$ (40)
1329	1329	1371	188.34	1994	$\upsilon_{CC\ Naphtq.}$ (57)
	1316	1364	31.14	264	$\rho_{HCCH\ Benz.}$ (77)
	1305	1348	5.51	5563	$\upsilon_{CC\ Naphtq.\ Asym} + \upsilon_{CC\ Benz.Asym.}$ (46)
1286		1318	624.32	1993	$\upsilon_{CC\ Naphtq.\ Asym.}$ (13); $\upsilon_{CC\ Benz.\ Asym.}$ (40)
	1255	1290	295.91	4458	$\upsilon_{CC\ Naphtq.} + \upsilon_{NC\ Naphtq.} + \upsilon_{CN\ Benz.}$ (26)
1240		1270	215.12	2296	$\upsilon_{CC\ Naphtq.\ Asym.}$ (15); $\delta_{HCC\ Naphtq.}$ (24)
1190	1193	1226	25.46	704	$\upsilon_{CC\ Naphtq.\ Asym.} + \upsilon_{NC\ Naphtq.\ Sym.} + \upsilon_{CN\ Benz.\ Sym.}$ (41)
1173	1174	1202	3.23	937	$\upsilon_{CC\ Naphtq.\ Asym.} + \upsilon_{CC\ Benz.\ Asym.}$ (12); $\delta_{HCC\ Benz.}$ (71)
1161	1164	1186	39.14	1385	$\delta_{HCC\ Naphtq.}$ (74)
	1153	1180	3.25	236	$\delta_{HCC\ Benz.}$ (71)
1140	1140	1169	144.27	3593	$\upsilon_{CC\ Naphtq.\ Asym.}$ (27); $\delta_{HCC\ Naphtq.}$ (13)
1089	1091	1124	1.18	194	$\rho_{HCCH\ Naphtq.}$ (30); $\delta_{CCC\ Naphtq.}$ (17)
1076		1115	34.39	346	$\upsilon_{CCBenz.\ Asym.}$ (35); $\rho_{HCCH\ Benz.}$ (37)
1047	1048	1062	24.12	262	$\upsilon_{CC\ Benz.}$ (43); $\delta_{CCC\ Benz.}$ (13); $\rho_{HCCH\ Benz.}$ (21)
1016	1017	1049	72.87	4998	$\upsilon_{CC\ Naphtq.}$ (39)
997	1002	1028	5.41	4739	$\upsilon_{CC\ Benz.}$ (24); $\delta_{CCC\ Benz.}$ (66)
982	977	1011	0.13	91	$\tau_{HCCH\ Benz.}$ (68); $\tau_{CCCC\ Benz.}$ (20)
921	925	956	26.66	503	$\omega_{HCC\ Benz.}$ (54)
899	898	930	8.32	729	$\delta_{CNC\ Benz.} + \delta_{CCN\ Naphtq.}$ (14); $\tau_{HCCH\ Benz.}$ (23)
	850	868	38.03	1306	$\omega_{HCCH\ Benz.}$ (46)
848		866	54.80	327	$\upsilon_{CCl\ Naphtq.}$ (13); $\omega_{HCCH\ Benz.}$ (44)
	810	823	0.35	248	$\tau_{HCCH\ Naphtq.}$ (10); $\omega_{CC=O\ Naphtq.} + \tau_{CCCC\ Naphtq.}$ (59)
800	801	821	34.13	258	$\omega_{CCC\ Benz.}$ (10)
789	792	789	69.38	268	$\omega_{HCCH\ Benz.}$ (58)
756		752	70.09	252	$\omega_{HCCH\ Naphtq.}$ (33); $\omega_{CC=O\ Naphtq.}$ (35)
717	722	720	62.40	71	$\omega_{HCCH\ Benz.}$ (40); $\tau_{CCCC\ Benz.}$ (50)
692	690	712	27.48	146	$\tau_{CCC\ Naphtq.}$ (11); $\tau_{CCN\ Naphtq.} + \tau_{CC=O\ Naphtq.}$ (37)
665	665	683	8.98	1174	$\delta_{CCC\ Naphtq.}$ (32)
640	643	650	10.37	2122	$\delta_{CCC\ Naphtq.}$ (11); $\delta_{CC=O\ Naphtq.} + \omega_{CCN\ Benz.}$ (12); $\omega_{CCC\ Benz.}$ (10)
624	627	636	8.68	3895	$\delta_{CCC\ Benz.}$ (58)
610	616	613	71.57	4150	$\delta_{CCC\ Naphtq.} + \delta_{CCC\ Benz.}$ (12); $\tau_{HNC\ Naphtq.}$ (32)

The percentage contributions of each coupled mode at the same frequency were indicated in parentheses. υ: stretching; δ: scissoring; ω: wagging; τ: twisting; σ: rocking; Sym.: symmetric; Asym.: antisymmetric; Benz.: benzene ring; Naphtq.: naphthoquinone ring; Subst.: substituents; PED: potential energy distribution.

Table 3. Experimental and theoretical vibrational wavenumbers of **1b**

Experimental wavenumber / cm^{-1}		Calculated wavenumber / cm^{-1}	IR intensity / cm^{-1}	Raman intensity / cm^{-1}	PED / %
Infrared	Raman				
3221	3228	3539	238.56	1401	$\upsilon_{NH\ Naphtq.}$ (100)
3062	3062	3206	13.16	811	$\upsilon_{CH\ Benz.\ Asym.}$ (91)
3030		3189	24.00	293	$\upsilon_{CH\ Benz.\ Asym.}$ (89)
2958		3136	23.91	458	$\upsilon_{CH\ Subst.\ Asym.}$ (100)
2921	2921	3111	25.67	541	$\upsilon_{CH\ Subst.\ Asym.}$ (99)
2852		3052	37.99	1553	$\upsilon_{CH\ Subst.\ Sym.}$ (99)
1674	1675	1781	329.78	8251	$\upsilon_{C=O\ Naphtq.}$ (85)
1633	1636	1752	285.53	13427	$\upsilon_{C=O\ Naphtq.}$ (81)
	1613	1693	21.50	15414	$\upsilon_{CC\ Benz.\ Asym.}$ (63); $\delta_{HCC\ Benz.}$ (16)
1593	1596	1672	245.42	2083	$\upsilon_{CC\ Naphtq.\ Sym.}$ (48)
1558	1563	1644	978.55	13802	$\upsilon_{CC\ Naphtq.\ Asym.}$ (53)
1515	1523	1578	836.90	4310	υ_{CN} (24); $\delta_{HNC\ Naphtq.}$ (33); $\delta_{HCC\ Benz.}$ (12)
1494		1562	133.29	313	$\delta_{HNC\ Naphtq.}$ (27); $\delta_{HCC\ Benz.}$ (32)
1459	1459	1536	59.98	169	$\delta_{CCC\ Naphtq.}$ (12); $\delta_{HCC\ Naphtq.}$ (53)
1410	1409	1494	44.90	367	$\delta_{H3CC\ Subs.}$ (23); $\tau_{HCH\ Subst.}$ (48)
1375	1378	1456	12.77	205	$\upsilon_{CC\ Benz.\ Asym.}$ (28); $\delta_{HCC\ Benz.}$ (26); $\tau_{HCC\ Subst.}$ (20)
1329	1326	1371	224.18	2698	$\upsilon_{CC\ Naphtq.\ Asym.}$ (40)
1311	1314	1344	8.23	5104	$\upsilon_{CCNaphtq.\ Asym.}$ (10); $\rho_{HCCH\ Benz.}$ (23)
1298	1303	1334	130.14	946	$\upsilon_{CC\ Naphtq.}$ (26); $\rho_{HCCH\ Benz.} + \rho_{HCCH\ Naphtq.}$ (12)
1284	1289	1315	632.59	2286	$\upsilon_{CC\ Naphtq.\ Asym.} + \upsilon_{CC\ Benz.\ Asym.}$ (47)
1240		1291	227.72	5013	$\upsilon_{CCNaphtq.\ Asym.} + \upsilon_{CC\ Benz.\ Asym.}$ (16); $\upsilon_{NC\ Benz.}$ (13)
	1212	1270	201.24	2201	$\upsilon_{CC\ Naphtq.\ Asym.}$ (12); $\delta_{HCC\ Naphtq.}$ (26)
1190	1191	1250	14.62	1046	$\upsilon_{CC\ Benz.Asym.} + \upsilon_{CH3\text{-}C\ Subst.}$ (53); $\delta_{HCC\ Benz.}$ (20)
1174	1176	1229	22.77	740	$\upsilon_{CC\ Benz.\ Sym.}$ (10); $\upsilon_{NC\ Naphtq.}$ (16); $\upsilon_{NC\ Benz.}$ (12)
1157	1160	1206	6.27	1726	$\delta_{HCCH\ Benz.}$ (72)
1140	1141	1170	140.70	3564	$\upsilon_{CC\ Naphtq.}$ (30)
1109		1144	29.81	108	$\upsilon_{CC\ Benz.\ Asym.}$ (22); $\delta_{HCCH\ Benz.}$ (63)
1047		1079	11.40	69	$\upsilon_{CC\ Naphtq.}$ (25); $\rho_{HCC\ Naphtq.}$ (21)
1018		1050	103.10	6412	$\upsilon_{CC\ Naphtq.\ Asym.}$ (50)
984		1027	1.32	4	$\tau_{HCCH\ Naphtq.}$ (78); $\omega_{CCCC\ Naphtq.}$ (11)
964	962	1016	1.35	138	$\tau_{HCH\ Subs.}$ (60); $\omega_{HCC\ Subst.}$ (11)
943	944	986	8.23	232	$\tau_{HCCH\ Benz.}$ (74)
914	915	940	27.23	1522	$\delta_{CCCl\ Naphtq.} + \delta_{CCN\ Naphtq.} + \delta_{CNC\ Naphtq.}$ (30)
848	852	872	65.57	1664	$\upsilon_{CC\ Benz.\ Sym.} + \upsilon_{CCl\ Naphtq.}$ (21); $\delta_{CCC\ Naphtq.}$ (16)
818	817	842	70.86	1245	$\upsilon_{CCl\ Naphtq.} + \upsilon_{CC\ Benz.\ Sym} + \upsilon_{CC\ Naphtq.\ Sym}$ (40)
804		829	15.42	131	$\omega_{HCCH\ Naphtq.}$ (45); $\omega_{CC=O\ Naphtq.}$ (28)
787		776	18.83	264	$\omega_{CCC\ Benz.} + \omega_{CCC\ Naphtq.}$ (14)
758	757	752	69.96	457	$\omega_{HCCH\ Naphtq.}$ (29); $\omega_{CC=O\ Naphtq.}$ (30)
	744	744	24.12	350	$\omega_{CNC\ Benz.} + \omega_{CCC\ Benz.}$ (20)
716	720	711	26.62	140	$\tau_{HCCH\ Naphtq.}$ (11); $\omega_{CCC\ Naphtq.}$ (18); $\tau_{CCC\ Naphtq.}$ (19)
679	674	682	11.17	1077	$\tau_{CCC\ Naphtq.} + \delta_{CCN\ Naphtq.} + \tau_{CNC\ Naphtq.} + \omega_{CCC\ Benz.} + \tau_{CCN\ Benz.}$ (23)
660	659	660	11.53	850	$\delta_{CCC\ Naphtq.} + \delta_{CCN\ Benz.}$ (61)
640	641	643	27.06	8255	$\delta_{CCC\ Naphtq.}$ (21); $\omega_{HNC\ Naphtq.}$ (21)
613	614	610	109.14	16578	$\omega_{HNC\ Naphtq.}$ (63)

The percentage contributions of each coupled mode at the same frequency were indicated in parentheses. υ: stretching; δ: scissoring; ω: wagging; τ: twisting; σ: rocking; Sym.: symmetric; Asym.: antisymmetric; Benz.: benzene ring; Naphtq.: naphthoquinone ring; Subst.: substituents; PED: potential energy distribution.

Table 4. Experimental and theoretical vibrational wavenumbers of **1c**

Experimental wavenumber / cm^{-1}		Calculated wavenumber / cm^{-1}	IR intensity / cm^{-1}	Raman intensity / cm^{-1}	PED / %
Infrared	Raman				
3247		3538	244.68	1409	$\upsilon_{NH\ Naphtq.}$ (100)
	3069	3233	11.05	1245	$\upsilon_{CH\ Naphtq.\ Sym.}$ (100)
	3048	3219	6.26	965	$\upsilon_{CH\ Benz.\ Asym.}$ (94)
3040		3217	7.93	791	$\upsilon_{CH\ Naphtq.\ Asym.}$ (90)
	3017	3205	3.42	448	$\upsilon_{CH\ Naphtq.\ Asym.}$ (92)
2960		3169	26.41	565	$\upsilon_{CH\ Subst.\ Asym.}$ (100)
2920		3107	44.54	316	$\upsilon_{CH\ Subst.\ Asym.}$ (100)
2852		3041	59.37	729	$\upsilon_{CH\ Subst.\ Sym.}$ (100)
1674	1675	1781	331.62	8358	$\upsilon_{C=O\ Naphtq.}$ (86)
1633	1636	1750	264.12	14394	$\upsilon_{C=O\ Naphtq.}$ (81)
	1610	1691	79.28	16254	$\upsilon_{CC\ Benz.}$ (58); $\delta_{CCH\ Benz.}$ (12)
1593	1592	1672	230.06	2445	$\upsilon_{CC\ Naphtq.}$ (61)
1564	1565	1643	968.97	14544	$\upsilon_{CC\ Naphtq.} + \upsilon_{CN\ Naphtq.}$ (56)
1514	1517	1578	1053.81	4028	$\delta_{HNC\ Benz.}$ (40); $\delta_{HCC\ Benz.}$ (10)
1493	1500	1560	181.45	406	$\delta_{HNC\ Benz.}$ (20); $\delta_{HCC\ Benz.}$ (37)
1454	1455	1536	57.24	148	$\delta_{HCC\ Naphtq.}$ (53); $\delta_{CCC\ Naphtq.}$ (14)
1439	1442	1505	58.98	356	$\delta_{HCH\ Subst.}$ (69); $\tau_{H3CO\ Subst.}$ (23)
1417	1419	1492	14.14	449	$\delta_{HCH\ Subst.}$ (71); $\tau_{H3CO\ Subst.}$ (22)
1328		1373	305.91	5685	$\upsilon_{CC\ Naphtq.\ Asym.}$ (52)
1311		1358	42.23	5984	$\upsilon_{CN\ Naphtq.\ Asym.} + \upsilon_{CC\ Benz.\ Asym.} + \upsilon_{CC\ Naphtq.\ Asym.} + \upsilon_{C\text{-}O\ Benz.\ Asym.}$ (49)
	1303	1340	31.50	2826	$\rho_{HCCH\ Naphtq.} + \rho_{HCCH\ Benz.}$ (41); $\upsilon_{CC\ Naphtq.\ Asym.}$ (12)
1284		1291	915.32	1107	$\upsilon_{CO\ Benz.} + \upsilon_{CC\ Benz.\ Asym.}$ (50); $\rho_{HCCH\ Benz.}$ (11)
	1268	1290	62.71	3507	$\upsilon_{CN\ Benz.} + \upsilon_{CC\ Benz.\ Asym.}$ (33); $\rho_{HCCH\ Naphtq.}$
1234	1241	1271	183.13	2275	$\upsilon_{CC\ Naphtq.\ Sym.}$ (17); $\delta_{HCC\ Naphtq.}$ (32)
1194	1193	1197	35.89	1920	$\upsilon_{CC\ Benz.\ Sym.}$ (12); $\delta_{HCC\ Benz.}$ (70)
1180	1172	1186	51.49	2237	$\delta_{HCC\ Naphtq.}$ (67)
1167		1171	127.01	3980	$\upsilon_{CC\ Naphtq.\ Sym.}$ (11); $\rho_{HCC\ Naphtq.}$ (14)
1140	1142	1138	52.46	252	$\upsilon_{CC\ Benz.\ Asym.}$ (14); $\rho_{HCC\ Benz.}$ (64)
1047		1082	90.73	73	$\upsilon_{CO\ Subst.}$ (51); $\rho_{HCCH\ Naphtq.}$ (10)
1028	1021	1050	97.77	6726	$\upsilon_{CC\ Naphtq.\ Sym.}$ (51)
970		979	5.17	323	$\tau_{HCCH\ Benz.}$ (68)
933	934	940	30.88	1653	$\upsilon_{CC\ Benz.\ Sym.}$ (12); $\delta_{CNC} + \delta_{CCN\ Naphtq.}$ (20)
	873	873	66.58	1271	$\upsilon_{CC\ Benz.\ Sym.}$ (13); $\delta_{CCC\ Naphtq.}$ (17); $\delta_{HCCC\ Benz.}$ (14)
848	855	842	118.47	1469	$\upsilon_{CC\ Benz.\ Sym.}$ (14); $\upsilon_{Cl\text{-}C\ Sym.}$ (15); $\delta_{CCC\ Benz.} + \delta_{CC=O\ Naphtq.}$ (13); $\delta_{CCC\ Naphtq.}$ (10)
829		829	14.15	171	$\tau_{HCC\ Naphtq.}$ (47); $\omega_{CCC=O}$ (27); $\omega_{CCCC\ Naphtq.}$ (10)
818	818	822	1.15	264	$\omega_{CC=O} + \omega_{CCC\ Naphtq.} + \tau_{HCC\ Naphtq.}$ (63)
789	788	782	4.43	134	$\tau_{CC=O} + \omega_{CCC\ Naphtq.} + \omega_{CCC\ Benz.}$ (18)
758	759	752	81.09	378	$\tau_{HCC\ Naphtq.}$ (28); $\omega_{O=CC}$ (33)
717	720	711	28.21	153	$\tau_{HCC\ Naphtq.}$ (10); $\tau_{CCN\ Naphtq.} + \omega_{CCC\ Naphtq.}$ (22); $\omega_{CCC\ Naphtq.}$ (11)
683		683	4.03	1332	$\delta_{CC=O\ Naphtq.} + \delta_{CCC\ Benz.} + \delta_{CCC\ Naphtq.}$ (28)
652	653	657	14.00	1219	$\delta_{CCC\ Benz.} + \delta_{CCC\ Naphtq.}$ (49); $\delta_{CC=O\ Naphtq.}$ (13)
	641	644	43.67	14535	$\delta_{CCC\ Naphtq.} + \omega_{CCC\ Benz.}$ (15); $\omega_{HNCC\ Benz.}$ (31)
609		617	85.27	13870	$\omega_{HNC\ Benz.}$ (49)

The percentage contributions of each coupled mode at the same frequency were indicated in parentheses. υ: stretching; δ: scissoring; ω: wagging; τ: twisting; σ: rocking; Sym.: symmetric; Asym.: antisymmetric; Benz.: benzene ring; Naphtq.: naphthoquinone ring; Subst.: substituents; PED: potential energy distribution.

Table 5. Experimental and theoretical vibrational wavenumbers of **1d**

Experimental wavenumber / cm^{-1}		Calculated wavenumber / cm^{-1}	IR intensity / cm^{-1}	Raman intensity / cm^{-1}	PED / %
Infrared	Raman				
3222	3228	3542	246.97	1363	$\upsilon_{NH\ Naphtq.}$ (100)
3085	3087	3233	13.00	1433	$\upsilon_{CH\ Naphtq.\ Sym.}$ (93)
3064	3067	3221	5.20	958	$\upsilon_{CH\ Benz.\ Sym.}$ (97)
	3054	3218	6.59	747	$\upsilon_{CH\ Naphtq.\ Asym.}$ (93)
3041	3043	3208	8.77	419	$\upsilon_{CH\ Benz.\ Asym.}$ (99)
2999	3002	3172	23.26	510	$\upsilon_{CH\ Subst.\ Asym.}$ (90)
2970	2969	3160	34.25	613	$\upsilon_{CH\ Subst.\ Asym.}$ (98)
2939	2936	3121	41.80	296	$\upsilon_{CH\ Subst.\ Asym.}$ (97)
2922		3112	40.11	282	$\upsilon_{CH\ Subst.\ Asym.}$ (99)
2848	2850	3045	49.55	1205	$\upsilon_{CH\ Subst.\ Sym.}$ (95)
2835	2836	3044	77.03	168	$\upsilon_{CH\ Subst.\ Asym.}$ (91)
1670	1671	1781	325.97	8125	$\upsilon_{C=O\ Naphtq.}$ (84)
1635	1636	1754	286.63	13334	$\upsilon_{C=O\ Naphtq.}$ (82)
	1609	1683	132.12	15910	$\upsilon_{CC\ Benz.}$ (56)
1593		1672	185.83	2134	$\upsilon_{CC\ Benz.}$ (11); $\upsilon_{CC\ Naphtq.}$ (43)
1564	1563	1644	955.73	11152	$\upsilon_{CC\ Naphtq.} + \upsilon_{CN\ Naphtq.}$ (36)
1520	1525	1573	877.30	1790	$\upsilon_{CN\ Benz.}$ (11); $\delta_{HNC\ Benz.}$(38)
1500	1501	1561	268.95	1212	$\upsilon_{C\text{-}O\ Benz.}$ (10); $\delta_{HNC\ Benz.}$ (25); $\delta_{HCC\ Benz.}$ (27)
1467		1508	14.42	270	$\upsilon_{CC\ Naphtq.}$ (15); $\delta_{HCC\ Naphtq.}$ (30); $\omega_{HCH\ Subt.}$ (16)
	1455	1507	78.72	531	$\delta_{HCC\ Naphtq.}$ (12); $\omega_{HCH\ Subt.}$ (38)
1446		1503	51.10	1159	$\delta_{HCH\ Subt.}$ (60); $\tau_{H3CO\ Subt.}$ (14)
1421	1422	1493	16.24	402	$\delta_{HCH\ Subt.}$ (16); $\tau_{H3CO\ Subt.}$ (76)
1331		1370	286.70	3345	$\upsilon_{CC\ Naphtq.\ Asym.}$ (50)
1294	1293	1336	205.46	1446	$\upsilon_{CC\ Naphtq.\ Asym.} + \upsilon_{CC\ Benz.\ Asym.}$ (43)
1284		1317	413.50	1545	$\upsilon_{CC\ Naphtq.\ Asym.} + \upsilon_{CC\ Benz.\ Asym.}$ (62)
1236	1235	1274	541.47	664	$\upsilon_{OC\ Benz.}$ (18); $\upsilon_{CC\ Benz.}$ (10); $\delta_{HCC\ Benz.}$ (13)
1221	1220	1262	81.30	1673	υ_{OCBenz} (22); $\delta_{HCC\ Naphtq.}$ (13)
1188		1222	27.56	292	$\delta_{HCO\ Subt.}$ (10); $\omega_{HCH\ Subt.}$ (50)
1157		1212	56.98	325	$\delta_{HCC\ Benz.}$ (10); $\omega_{HCH\ Subt.}$ (51)
1130	1133	1185	58.45	1863	$\delta_{HCC\ Naphtq.}$ (68)
1043	1041	1077	64.94	358	$\upsilon_{CO\ Subst.}$ (60); $\rho_{HCCH\ Benz.}$ (19)
1026		1053	142.41	2085	$\upsilon_{CO\ Subst.}$ (64)
	1019	1049	71.11	4928	$\upsilon_{CC\ Naphtq.\ Sym.}$ (30); $\upsilon_{CO\ Subst.}$ (11); $\delta_{CC=O\ Naphtq.}$ (14)
973	975	1003	55.02	726	$\upsilon_{CC\ Benz.}$ (24)
881		891	40.77	183	$\delta_{CCC\ Naphtq.} + \delta_{CCO\ Naphtq.} + \delta_{CCN\ Naphtq.}$ (10); $\omega_{HCC\ Benz.}$ (65)
854		854	95.73	519	$\upsilon_{Cl\text{-}C\ Sym.} + \upsilon_{CC\ Naphtq.}$ (46); $\delta_{CCC\ Naphtq.} + \delta_{CCC\ Benz.}$ (15)
831		829	14.28	202	$\omega_{HCCC\ Naphtq.}$ (49); $\tau_{CCCC\ Naphtq.}$ (36)
802		802	3.52	1082	$\upsilon_{O\text{-}C\ Benz.}$ (17); $\tau_{CCC\ Benz.}$ (22)
769		773	29.44	2948	$\upsilon_{CC\ Benz.}$ (12); $\omega_{CCC\ Benz.} + \omega_{CCC\ Naphtq.}$ (13)
748	749	749	53.18	178	$\tau_{HCC\ Naphtq.}$ (23); $\omega_{CC=O\ Naphtq.}$(25)
719	719	711	25.43	166	$\omega_{CCC\ Naphtq.}$ (16); $\omega_{CC=O\ Naphtq.}$ (38)
685	685	688	12.12	1067	$\delta_{CCC\ Naphtq.} + \omega_{CC=O\ Naphtq.} + \tau_{CCC\ Benz.}$ (14)
654	651	660	25.71	911	$\delta_{CCC\ Naphtq.}$ (34); $\omega_{CCC\ Benz.}$ (12)
634	634	626	22.86	1823	$\omega_{CCC\ Benz.}$ (24)

The percentage contributions of each coupled mode at the same frequency were indicated in parentheses. υ: stretching; δ: scissoring; ω: wagging; τ: twisting; σ: rocking; Sym.: symmetric; Asym.: antisymmetric; Benz.: benzene ring; Naphtq.: naphthoquinone ring; Subst.: substituents; PED: potential energy distribution.

in Figure 7 was classified as the region associated with the N–H stretching mode. The Raman spectrum showed a single band of low intensity between 3250 and 3220 cm^{-1}. The infrared spectra of the solid phase have a medium intensity broadband indicating the influence of intermolecular interactions, particularly hydrogen bonding. This profile confirms the presence of the secondary aromatic amino group. Due to the presence of the hydrogen bonds in the crystal packing, this band was not included in the calculation of the scale factor mentioned in the previous item.

Aromatic C–H stretching modes were observed for all compounds in the region between 3040 and 3100 cm^{-1}. The asymmetric and symmetric aromatic ν_{CH} modes (benzenoid and naphthoquinone groups) were assigned. The methoxylated compounds **1c** and **1d** showed the lower definition of these bands in the infrared spectra. Stretching modes of the aliphatic C–H bonds were observed in the region between 2850 and 3000 cm^{-1}. The theoretical information and the differences between the vibrational modes were essential in the assignment of these bands, due to the spectra complexity in this region. Bands in 2958, 2921 and 2852 cm^{-1} were identified in **1b** and **1c** as asymmetric and symmetric ν_{CH} modes. In the spectrum of derivative **1d**, a larger number of bands is noticed, reflecting the increase in the number of methoxy groups.

Region between 1800-1300 cm^{-1}

Bands of high intensity due to $\nu_{C=C}$, $\nu_{C=O}$ and ν_{CN} modes and coupled stretching modes were observed in the experimental spectra between 1670 and 1450 cm^{-1}, as shown in Figure 7. In infrared spectra, $\nu_{C=O}$ modes in the naphthoquinone group were identified in two bands at 1675/1670 and 1635/1633 cm^{-1}. The $\nu_{C=C}$ modes of the aromatic groups were observed in the 1593 cm^{-1} as a high intensity band. The band at 1564/1558 cm^{-1} was assigned as a coupled mode of $\nu_{C=C}$ and ν_{CN}, followed by bands at 1520 and 1500 cm^{-1} that have been associated with HCC and HNC angle strain coupling modes. In the Raman spectra, these bands are observed, but especially on the band at 1636/1635 cm^{-1} as $\nu_{C=O}$ modes. These data reinforce the similarity of the four compounds with their benzenoid and naphthoquinone groups.

Region between 1300-1000 cm^{-1}

The region between 1285 and 1130 cm^{-1} shows greater complexity for the spectrum in Figure 7 containing the two methoxy groups compared to the other systems studied. The compound **1d** presents an envelope of bands where the most intense band is found at 1236 cm^{-1} associated with the coupling $\nu_{C\text{-}O\text{-}CH3}$, ν_{CC} and $\nu_{HCC\ Benz}$. This compound still presents intense bands at 1284 and 1130 cm^{-1} that are associated with ν_{CC} and $\nu_{CCH\ Naphtq.}$ modes. These two bands are the most prominent among the other compounds. Even though the **1c** substance contains the methoxy group, it has been identified as participating in the coupled mode at 1284 cm^{-1}. In the Raman spectra, the band at 1255 cm^{-1} was highlighted for the compounds **1a** and **1b**, assigned as $\nu_{CC} + \nu_{CN}$ mode and presents in both aromatic groups. For the compounds **1c** and **1d**, this intense band is observed at 1268 and 1293 cm^{-1}.

Region between 1000-600 cm^{-1}

The infrared spectrum in Figure 7 for the compound **1d** reinforces the distinction between the compounds according to the highest number of substituents present. The characteristic region of aromatic rings respiration and deformation outside the plane was observed with bands at 854, 831 802, 748, 719, 685 and 654 cm^{-1}. Furthermore, the first highlighted band is assigned by coupling the breathing mode of the aromatic rings with the ν_{CCl}. For the other compounds **1a**-**1c**, this mode stands out as a band of medium intensity found in the other compounds at 848/818 cm^{-1}, in addition to the out-of-plane deformation of the aromatic rings at 717/715 cm^{-1}. In the Raman spectrum, this region stands out for a band of weak intensity between 686 and 653 cm^{-1} related to the δ_{CCC} angular deformation of the aromatic rings.

Region between 600-150 cm^{-1}

As previously discussed, this region presents a great complexity, as it presents several active bands for all compounds in Figure S2 in the SI section. However, this region allows for greater differentiation between the compounds through the profile and intensity of the bands, also featuring a fingerprint region to distinguish these compounds. However, the intense band between 390 and 382 cm^{-1} stands out in all compounds for describing the out-of-plane deformation of aromatic rings with low intensity bands between 360 and 331 cm^{-1} which is assigned by the coupling of $\nu_{CC} + \nu_{CCl} + \delta_{CC=O}$. In the Raman spectrum, the band between 296 and 283 cm^{-1} is an indication for all compounds as $\tau_{CCC\ Naphtq.} + \tau_{CCN\ Naphtq.} + \tau_{CCCl\ Naphtq.}$

Electronic spectra

The compounds **1a**-**1d** listed in this study show a color that ranges from purple to black in solid state, which in solution with the indicated solvents shows a red-orange color, typical of dyes containing anthraquinone groups.[61] The experimental UV-Vis spectra for different compounds and in different solvents show high similarity, as observed

in other studies containing aminoquinones.[23] All the spectra in the solution presented a lower intensity band in the visible region between 470 and 500 nm, which was responsible for a bluish-green to blue-green absorption that justifies the colors observed in solution[62,63] presented in Figure 8. This spectral region is similar to the study observed by Rajalakshmi *et al.*[54] with an aqueous *N*-(2-hydroxyethyl) piperazine-*N*'-(2-ethanesulfonic acid (HEPES) buffer:*N*,*N*-dimethylformamide (DMF) (2:8 v/v) solution. In the spectra in the ultraviolet region, two bands are observed: the first, a low-intensity band between 320 and 335 nm, and the second, a high-absorptivity band ranging from 275 to 283 nm. Using acetonitrile as a solvent, the highlighted spectrum obtained presents a medium intensity band ranging from 228 to 240 nm, which is not defined for the other solvents due to their transparency regions. When evaluating the solid-state spectra in Figure S4 in the SI section, a very broad and intense band is noticeable between 400 and 700 nm in the visible region and a more defined band in the ultraviolet region between 277 and 292 nm. The characteristics of the first band may explain the reason for the color variation observed in the solid state, since there is an overlap of multiple absorption bands in this region influenced by crystal packing with multiple intermolecular interactions.

The deconvolution spectra were obtained using different Gaussian numbers; five for acetonitrile, four for dichloromethane, and three for DMSO. Some bands were estimated at below 200 nm to aid in the deconvolution process. The overall-fit parameters and the molar absorptivities are presented in Table S14 of the SI section. Notably, all compounds **1a-1d** have molar absorptivity values at around 10^4 in the UV region and 10^3 in the visible. When assessing the visible band with the different solvents, a bathochromic effect accompanied by a hypochromic effect is observed when comparing these bands in acetonitrile/CH_2Cl_2 to DMSO. This can be explained by the difference in polarity between these solvents and the aromatic groups. Another relevant effect related to this band was the solvent-independent bathochrome shift used in ascending order for the compounds **1a** < **1b** < **1c** < **1d**. This demonstrates an effect of the different substituents as highlighted in the charge analysis, as it should also be observed in the HOMO-LUMO boundary orbitals that will be evaluated in the next section. When evaluating the values of molar absorptivity, we can infer a strong participation of $\pi \rightarrow \pi*$ transitions to the intense band in the ultraviolet region and $n \rightarrow \pi*$ in the visible region with the effect of a donor substituent such as methoxy containing isolated electron pairs that generate a known bathochromatic effect on the transitions. There is also the participation of auxochromic groups present in naphthoquinone that has a profile resembling *p*-benzoquinone[28,64] but is difficult to predict without an analysis of orbitals and electronic excitations as reported by Pereira-da-Silva *et al.*[28]

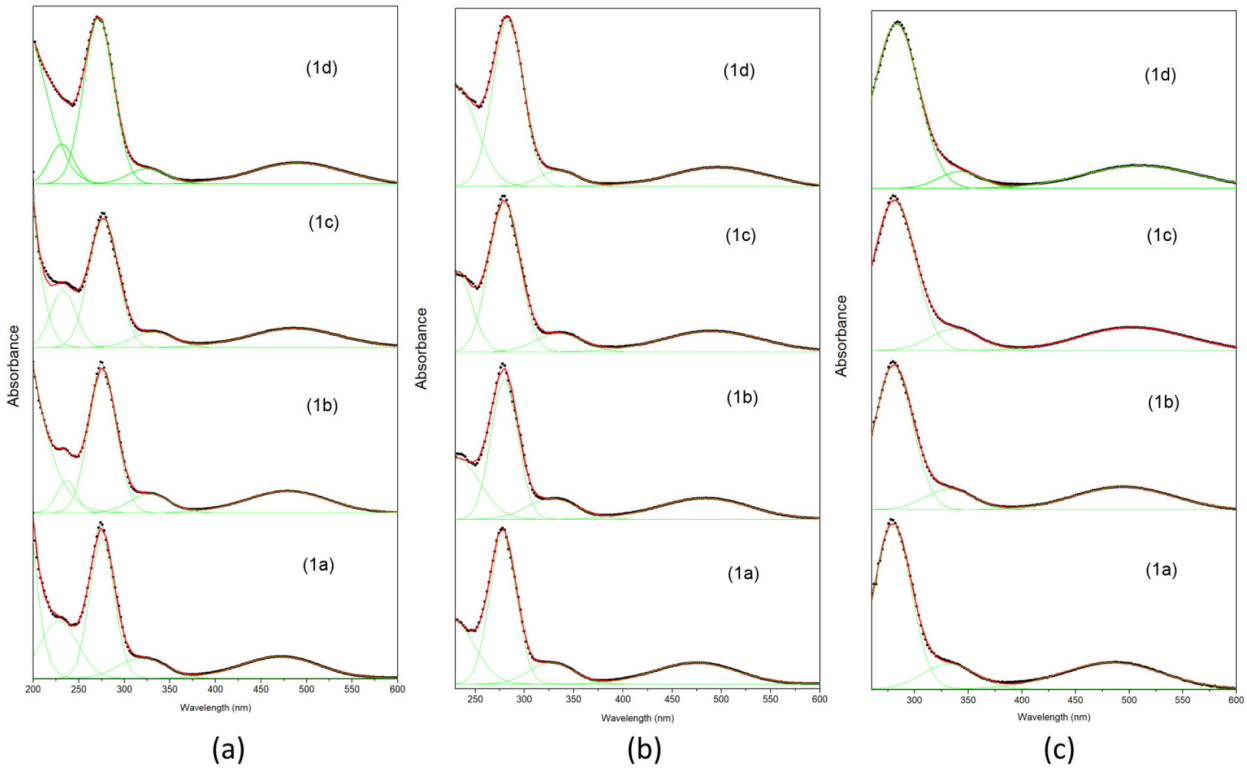

Figure 8. UV-Vis spectra (200 to 600 nm) in (a) acetonitrile, (b) dichloromethane, and (c) DMSO for the compounds **1a-1d**.

Molecular orbitals analysis

The ground state for all compounds **1a-1d** consists of the frontier region of occupied molecular orbitals distributed between 7 and 12 eV for CAM-B3LYP. Table 6 briefly presents these orbitals in an IEFPCM (solvent MeCN) with the associated Koopmans' energy and Mulliken analysis of the virtual and occupied orbitals. Five occupied orbitals and five virtual ones with lower energy were analyzed for **1c** and **1d**, while for the other compounds five occupied orbitals and eleven virtual ones with lower energy are highlighted. HOMO, LUMO, and other molecular orbitals of compounds are shown in Figure 9. The same analysis performed for the data obtained with the IEFPCM model with CH_2Cl_2 and DMSO is found in the SI section in Tables S15 and S16.

According to Borges *et al*.,[65] through DFT calculations it is feasible to predict the cytotoxic or cytoprotective effect of quinones by redox mechanism. For this, it is possible to use as a parameter the energy of the molecular orbitals HOMO and LUMO of compounds **1a-1d**, whose values are shown in Table 6. It is generally observed that quinones that exhibit higher εHOMO have the ability to donate electrons more easily, being carriers of cytoprotective properties. On the other hand, substances with high εLUMO imply electron acceptor molecules, which have cytotoxic properties. Thus, it can be noted that the quinones **1a-1d** studied in this work, especially the compounds **1b** and **1c-1d**, which contain electron-donating substituents by the electron-donating inductive effect and by the resonance effect, respectively, have high values of εHOMO and low values of εLUMO. These results indicate a greater capacity to donate electrons and, therefore, having probable cytoprotective effects.[66]

Based on Koopman's theorem, it is worth mentioning that the HOMO-LUMO energy difference for the compounds fluctuates from 5.48 to 5.23 eV in solvent

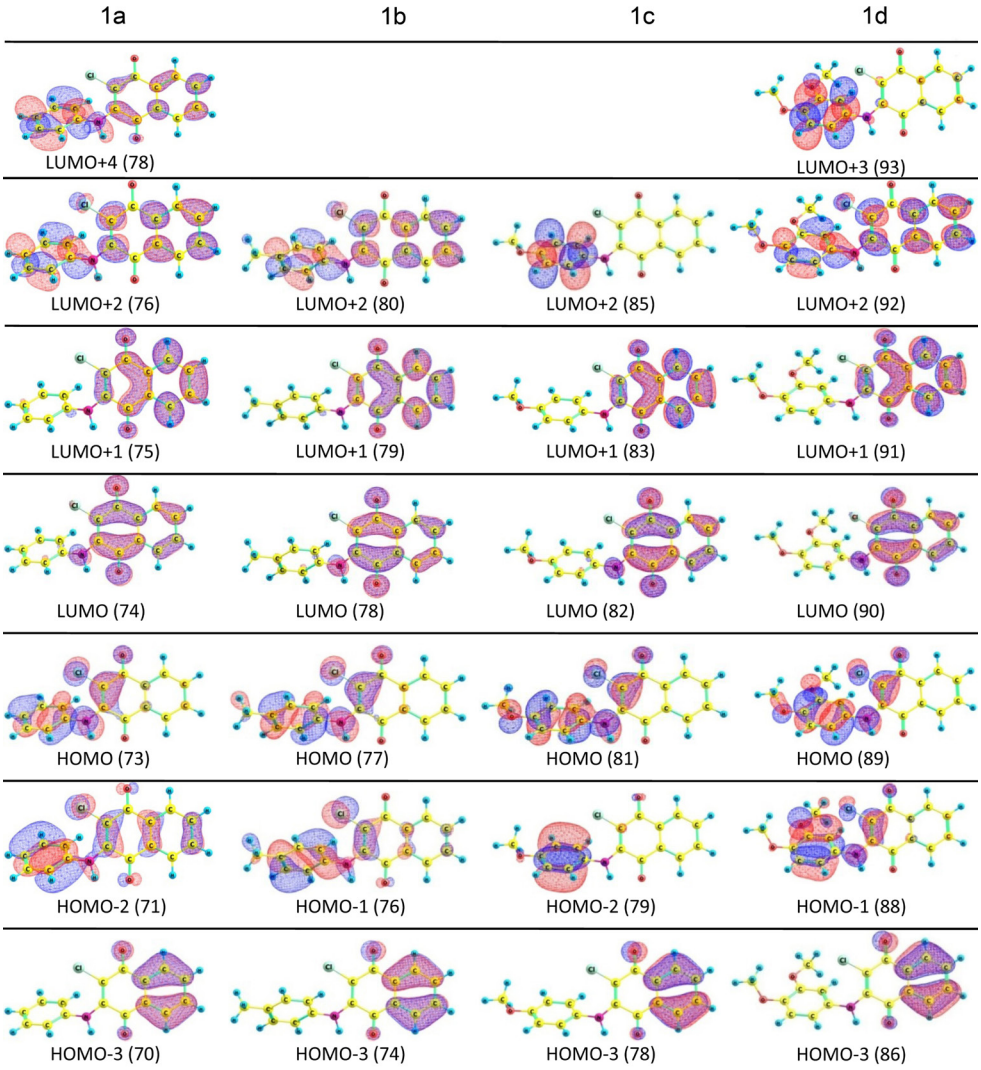

Figure 9. Orbital representation at the CAM-B3LYP level of compounds **1a-1d**. The contour values of the orbitals are all 0.03 a.u.

Table 6. Koopmans' energy, Mulliken population analysis and assignment for the frontier orbitals of **1a-1d** of the CAM-B3LYP method

Orbital	Energy / eV	Mulliken population	Energy / eV	Mulliken population
		1a		**1b**
L+4	1.16	$\pi^*C{=}C_{Benz.}$ + $\pi^*C{=}C_{Naphtq.}$ (6% of NH; 58% of Benz.; 36% of Naphtq.)	1.19	$\pi^*C{=}C_{Benz.}$ + $\pi^*C{=}C_{Naphtq.}$ (6% of NH; 57% of Benz.; 33% of Naphtq.)
L+3	0.77	$\pi^*C{=}C_{Benz.}$ (99% of Benz.)	0.78	$\pi^*C{=}C_{Benz.}$ (97% of Benz.)
L+2	0.41	$\pi^*C{=}C_{Naphtq.}$ + $\pi^*C{=}C_{Benz.}$ (32% of Benz.; 66% of Naphtq.)	0.45	$\pi^*C{=}C_{Naphtq.}$ + $\pi^*C{=}C_{Benz.}$ (29% of Benz.; 68% of Naphtq.)
L+1	–0.15	$\pi^*C{=}C_{Naphtq.}$ (97% of Naphtq.)	–0.13	$\pi^*C{=}C_{Naphtq.}$ (97% of Naphtq.)
LUMO*	–2.10	$\pi C{=}C_{Naphtq.}$ + nO (94% of Naphtq.)	–2.08	$\pi C{=}C_{Naphtq.}$ + nO (94% of Naphtq.)
HOMO*	–7.58	$\pi C{=}C_{Benz.}$ + $\pi C{=}C_{Naphtq.}$ + nO + nCl + nN (24% of NH; 34% of Benz.; 43% of Naphtq.)	–7.47	$\pi C{=}C_{Benz.}$ + $\pi C{=}C_{Naphtq.}$ + nO + nCl + nN (22% of NH; 39% of Benz.; 37% of Naphtq.)
H-1	–8.69	$\pi C{=}C_{Benz.}$ + nCl (87% of Benz.; 13% of Naphtq.)	–8.59	$\pi C{=}C_{Benz.}$ + nCl + $\pi C{=}C_{Naphtq.}$ (64% of Benz.; 31% of Naphtq.)
H-2	–8.90	$\pi C{=}C_{Benz.}$ + $\pi C{=}C_{Naphtq.}$ + nCl (59% of Benz.; 39% of Naphtq.)	–8.76	$\pi C{=}C_{Benz.}$ + $\pi C{=}C_{Naphtq.}$ (79% of Benz.; 18% of Naphtq.)
H-3	–9.08	$\pi C{=}C_{Naphtq.}$ (99% of Naphtq.)	–9.07	$\pi C{=}C_{Naphtq.}$ (100% of Naphtq.)
H-4	–9.30	$\pi C{=}C_{Naphtq.}$ + nO (95% of Naphtq.)	–9.28	$\pi C{=}C_{Naphtq.}$ + nO (97% of Naphtq.)
H-5	–9.38	nO + $\sigma C{-}C_{Naphtq.}$ (5% of Benz.; 94% of Naphtq.)	–9.34	nO + $\sigma C{-}C_{Naphtq.}$ (97% of Naphtq.)
H-6	–10.00	nO + $\sigma C{-}C_{Naphtq.}$ (98% of Naphtq.)	–9.99	nO + $\sigma C{-}C_{Naphtq.}$ (98% of Naphtq.)
H-7	–10.63	nCl + $\sigma C{-}C_{Naphtq.}$ (5% of Benz.; 92% of Naphtq.)	–10.58	nCl + $\sigma C{-}C_{Naphtq.}$ (8% of Benz.; 90% of Naphtq.)
H-8	–10.99	nCl + $\pi C{=}C_{Benz.}$ (13% of NH; 41% of Benz.; 46% of Naphtq.)	–10.84	nCl + $\pi C{=}C_{Benz.}$ (14% of NH; 37% of Benz.; 44% of Naphtq.)
H-9	–11.53	nCl + $\sigma C{-}C_{Benz.}$ (77% of Benz.; 21% of Naphtq.)	–11.31	$\sigma C{-}C_{Naphtq.}$ + nCl + $\sigma C{-}H$ (74% of Benz.; 11% of Naphtq.; 12% of CH_3)
H-10	–11.76	nCl + $\pi C{=}C_{Naphtq}$+ $\pi C{=}O$ + $\sigma C{-}C_{Benz.}$ (8% of NH; 32% of Benz.; 59% of Naphtq.)	–11.59	$\sigma C{-}C_{Benz.}$ + $\sigma C{-}H$ (62% of Benz.; 9% of Naphtq.; 26% of CH_3)
		1c		**1d**
L+4	1.33	$\pi^*C{=}C_{Benz.}$ + $\pi^*C{=}C_{Naphtq.}$ (5% of NH; 66% of Benz.; 25% of Naphtq.)	1.24	$\pi^*C{=}C_{Benz.}$ + $\pi^*C{=}C_{Naphtq.}$ (6% of NH; 60% of Benz.; 28% of Naphtq.)
L+3	0.69	$\pi^*C{=}C_{Benz.}$ (98% of Benz.)	0.95	$\pi^*C{=}C_{Benz.}$ (90% of Benz.; 6% of Naphtq.)
L+2	0.55	$\pi^*C{=}C_{Naphtq.}$ + $\pi^*C{=}C_{Benz.}$ (20% of Benz.; 76% of Naphtq.)	0.44	$\pi^*C{=}C_{Naphtq.}$ + $\pi^*C{=}C_{Benz.}$ (28% of Benz.; 69% of Naphtq.)
L+1	–0.11	$\pi^*C{=}C_{Naphtq.}$ (98% of Naphtq.)	–0.14	$\pi^*C{=}C_{Naphtq.}$ (97% of Naphtq.)
LUMO*	–2.06	$\pi C{=}C_{Naphtq.}$ + nO + nN (94% of Naphtq.)	–2.10	$\pi C{=}C_{Naphtq.}$ + nO (94% of Naphtq.)
HOMO*	–7.29	$\pi C{=}C_{Benz.}$ + $\pi C{=}C_{Naphtq.}$ + nO + nCl + nN (16% of NH; 45% of Benz.; 12% of OCH_3; 27% of Naphtq.)	–7.33	$\pi C{=}C_{Benz.}$ + $\pi C{=}C_{Naphtq.}$ + nO + nCl + nN (15% of NH; 48% of Benz.; 25% of Naphtq.; 5% of OCH_3; 7% of OCH_3)
H-1	–8.31	$\pi C{=}C_{Benz.}$ + nO + nCl + nN (10% of NH; 30% of Benz.; 11% of OCH_3; 49% of Naphtq.)	–8.14	$\pi C{=}C_{Benz.}$ + nO + nCl + $\pi C{=}C_{Naphtq.}$ (8% of NH; 52% of Benz.; 22% of Naphtq.; 18% of OCH_3)
H-2	–8.85	$\pi C{=}C_{Benz.}$ (95% of Benz.)	–8.61	$\pi C{=}C_{Benz.}$ + nO + nCl (53% of Benz.; 35% of Naphtq.; 9% of OCH_3)
H-3	–9.06	$\pi C{=}C_{Naphtq.}$ (100% of Naphtq.)	–9.07	$\pi C{=}C_{Naphtq.}$ (100% of Naphtq.)
H-4	–9.26	$\pi C{=}C_{Naphtq.}$ + nO (97% of Naphtq.)	–9.28	$\pi C{=}C_{Naphtq.}$ (95% of Naphtq.)

Benz.: benzene ring; Naphtq.: naphthoquinone ring; n: isolated pair.

acetonitrile and is very close to the other results obtained for the other two-solvent systems. A relevant observation is that the highest barriers are found for compounds **1a**, without a *para* substituent on the benzene ring, **1b** with a methyl substituent (5.39 eV) and the lowest for compounds **1c** and **1d** with methoxy substituents. Such values are compatible with the inverse order of the activation strength of the substituents on phenyl group, where more activating groups tend to make the species more reactive to the detriment of less activating groups.

Orbitals close to the HOMO-LUMO border of H-3, H-2 through L+1 are characterized by the participation of orbitals associated with $\pi C{=}C_{Benz.}$ and $\pi C{=}C_{Naphtq}$ and isolated pairs of oxygen (carbonyl), nitrogen (amino) and chlorine (halogen) atoms. Specifically, for methoxy groups, orbitals where the most relevant participation exists for these groups are found in regions farther away from the HOMO-LUMO boundary orbitals. The electronic density of states (DOS) revealed that variations in the presence of substituent groups are found in the upper and lower energy ranges, different from those observed for the orbitals near the HOMO-LUMO border (Figure 10). This analysis confirms the similarity of the boundary orbitals, indicating the dominance of the benzenoid group orbital in HOMO and the naphthoquinonic group in LUMO. These trends are also reproduced in data with IEFPCM in CH_2Cl_2 and DMSO, with the results shown in Figures S5 and S6 of the SI section. This analysis confirms the observation highlighted by Rajalakshmi *et al.*[54] that intramolecular charge transfer (ICT) occurs from the benzenoid group to the quinone ring.

Electronic transitions

The first 50 singlet electronic excited states were calculated through the TD-CAM-B3LYP method. The observation of spin-allowed $\pi \rightarrow \pi^*$ transitions was the major concern in this work; therefore, the calculations were restricted to singlet states. All calculations were carried out without symmetry and with ground-state orbitals, to obtain the oscillator strength between the ground state and all excited states. The results of the energy and oscillator strength of the main calculated transitions are listed in Table 7, using the IEFPCM, with MeCN solvent. Tables S17 and S18 show the calculated excited states for IEFPCM with CH_2Cl_2 and DMSO (SI section). All calculations presented the first transition with a monoreferential nature and a dominant configuration

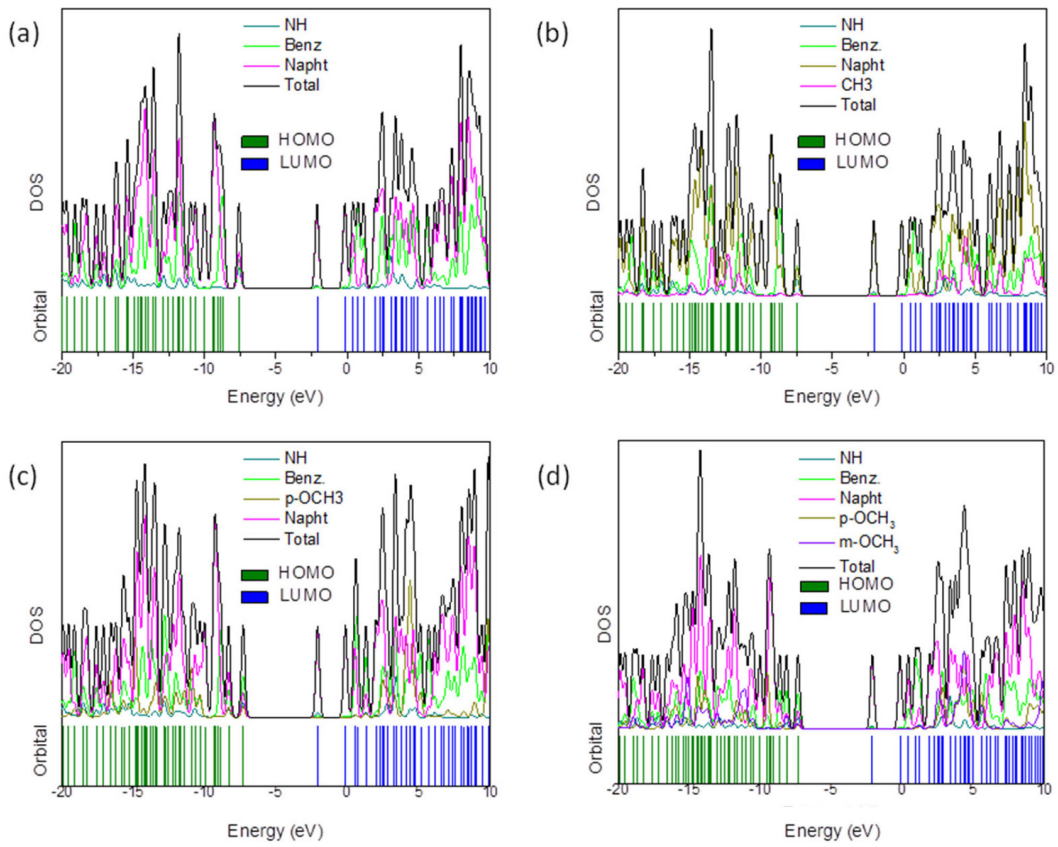

Figure 10. Energy level diagrams of compounds (a) **1a**, (b) **1b**, (c) **1c**, and (d) **1d** with SCF molecular orbitals within the CAM-B3LYP method and density orbital states (DOS) analysis.

coefficient involving the HOMO-LUMO orbitals. The states obtained in the ultraviolet region presented a multiconfigurational nature according to the values of the configuration interaction coefficients. By comparing the experimental results with the calculated excitations with proportional oscillator strengths, it can be seen that variations of less than 0.5 eV were observed in the calculations for the first bands in the UV-Vis spectra for the CAM-B3LYP orbitals regardless of the solvent used.

Concerning the experimental observations and theoretical results, the final assignments of the UV-Vis spectra electronic transitions are summarized in Table 8. The first transitions of each case are associated with the following assignments $\pi C{=}C_{Benz.} + \pi C{=}C_{Naphtq.} + nO + nCl + nN \rightarrow \pi C{=}C_{Naphtq.} + nO$. In other words, the influence of chromophore groups is confirmed in this band, without the participation of orbitals that indicate the presence of methyl or methoxy groups. However, single paired substituents are noted here. The other bands follow this trend, highlighting the nature of the transition $\pi \rightarrow \pi^*$ with a multiconfigurational nature in some transitions.

These results are compatible with several studies already carried out with different methods, such as semi-empirical, *ab initio* and DFT, for structures containing quinone groups with benzoquinone and its functionalized derivatives.[23,28]

Conclusions

The synthesis and theoretical-experimental characterization of the four 2-chloro-3-(phenylamino)-1,4-naphthoquinone derivatives presented in this work allowed corroborating and extending the observations highlighted in other studies for this compound class reported in the literature. Specifically, in this work, the combination of structural analysis by X-ray diffraction with the presentation of a new structure and associated with a broad theoretical discussion about the factors influencing the molecular characteristics enabled us to confirm the relevance of the intermolecular forces present in these derivatives. The analysis of the solid-phase vibrational and electronic spectra described in this article corroborated the analysis of the charge distribution, the presence of electronegative functional groups, and the study of the potential energy surface. Furthermore, the success in the spectroscopic assignment based on the isolated molecular units with the application of the implicit solvation model confirmed that such structures can show the maintenance of these conformations. Such

Table 7. Main singlet transition energies and oscillator strength from the ground state for compounds **1a-1d**, for TD-CAM-B3LYP/IEFPCM (solvent MeCN)

Band	Dominant configuration[a]	Energy / eV	f[b]	Dominant configuration[a]	Energy / eV	f[b]
	1a			**1b**		
1	73→74 (0.90)	2.95	0.1088	77→78 (0.88)	2.92	0.1174
2	70→74 (0.89)	4.27	0.0918	73→78 (0.15); 75→78 (0.12); 76→78 (0.52)	4.23	0.1136
	69→74 (0.16); 71→74 (0.38); 72→74 (0.31)	4.33	0.1565	74→78 (0.90)	4.28	0.1132
3	69→74 (0.18); 71→74 (0.15); 72→74 (0.53)	4.74	0.0688	73→78 (0.20); 75→78 (0.39); 76→78 (0.27)	4.72	0.0618
	68→74 (0.18); 69→74 (0.37); 71→74 (0.24)	4.96	0.1216	72→78 (0.11); 73→78 (0.44); 75→78 (0.29)	4.89	0.1299
	73→75 (0.64); 73→76 (0.17)	5.14	0.6736	77→79 (0.63); 77→80 (0.17)	5.11	0.7351
4	69→75 (0.40); 70→76 (0.10); 71→75 (0.13)	5.98	0.0751	70→78 (0.86)	5.79	0.0425
	70→75 (0.15); 72→77 (0.15);	6.30	0.1614	73→79 (0.44); 74→80 (0.10)	5.97	0.0822
	73→78 (0.30); 73→79 (0.12)			74→79 (0.26); 77→82 (0.20)	6.25	0.1940
	65→74 (0.14); 72→76 (0.15); 73→77 (0.22)	6.44	0.1247			
5	63→74 (0.17); 70→76 (0.17)	7.00	0.3575	66→78 (0.22); 76→80 (0.12)	6.97	0.3459
	71→75 (0.16); 71→77 (0.22); 72→77 (0.13)	7.18	0.2862	66→78 (0.18); 73→79 (0.13); 74→80 (0.24)	6.97	0.3737
	1c			**1d**		
1	80→82 (0.16); 81→82 (0.81)	2.89	0.1194	88→90 (0.14); 89→90 (0.77)	2.90	0.1140
2	75→82 (0.46); 76→82 (0.14); 80→82 (0.22)	3.86	0.0222	82→90 (0.20); 88→90 (0.47); 89→90 (0.14)	4.04	0.0328
	75→82 (0.32); 80→82 (0.41)	4.07	0.0623	86→90 (0.90)	4.27	0.1000
	78→82 (0.89)	4.28	0.1012	85→90 (0.10); 87→90 (0.58); 88→90 (0.24)	4.36	0.0705
3	77→82 (0.61); 79→82 (0.12)	4.76	0.1479	85→90 (0.70); 87→90 (0.11)	4.82	0.1818
	77→82 (0.13); 79→82 (0.34); 81→85 (0.36)	4.89	0.0695	89→91 (0.33); 89→92 (0.28); 89→93 (0.19)	5.03	0.5669
	79→82 (0.19); 81→83 (0.40); 81→85 (0.16)	5.08	0.4993	89→L+1 (0.24); 89→93 (0.37)	5.17	0.1955
4	77→83 (0.41); 80→83 (0.12)	5.94	0.1025	85→91 (0.16); 89→94 (0.21)	5.90	0.0859
	73→82 (0.31); 74→82 (0.18); 78→83 (0.23)	6.18	0.1264	85→91 (0.34); 89→94 (0.12)	5.98	0.0999
	73→82 (0.12); 78→83 (0.33); 81→86 (0.12)	6.25	0.1689	86→91 (0.45)	6.19	0.1154
				88→91 (0.11); 88→92 (0.13);	6.29	0.1615
				88→93 (0.16); 89→93 (0.20)		
5	76→84 (0.17); 79→85 (0.29); 80→84 (0.14)	6.83	0.3770	85→91 (0.17); 86→92 (0.34)	7.05	0.3516

[a]CI weights to the orbital list, shown in Table 6; [b]oscillator strength.

Table 8. Assignment of the electronic transitions at the CAM-B3LYP level for the compounds **1a-1d**

Peak	Wavelength / nm			Assignment	
	MeCN	CH_2Cl_2	DMSO		
				1a	
1	470	473	484	$\pi C{=}C_{Benz.} + \pi C{=}C_{Naphtq.} + nO + nCl + nN \rightarrow \pi C{=}C_{Naphtq.} + nO$	
2	319	327	332	$\pi C{=}C_{Naphtq.} \rightarrow \pi C{=}C_{Naphtq.} + nO$	$\pi C{=}C_{Benz.} + \pi C{=}C_{Naphtq.} + nCl \rightarrow \pi C{=}C_{Naphtq.} + nO$
3	275	278	279	$\pi C{=}C_{Naphtq.} + nO \rightarrow \pi C{=}C_{Naphtq.} + nO$	$\pi C{=}C_{Benz.} + \pi C{=}C_{Naphtq.} + nO + nCl + nN \rightarrow \pi^{*}C{=}C_{Naphtq.}$
4	228	225[a]		$\pi C{=}C_{Benz.} + \pi C{=}C_{Naphtq.} + nO + nCl + nN \rightarrow \pi C{=}C_{Naphtq.} + nO$	$\pi C{=}C_{Benz.} + \pi C{=}C_{Naphtq.} + nO + nCl + nN \rightarrow \pi^{*}C{=}C_{Benz.}$
5	167[a]			$\pi C{=}C_{Naphtq.} \rightarrow \pi C{=}C_{Benz.} + \pi C{=}C_{Naphtq.} + nCl$	$\pi C{=}C_{Benz.} + \pi C{=}C_{Naphtq.} + nCl \rightarrow \pi^{*}C{=}C_{Benz.}$
				1b	
1	478	482	494	$\pi C{=}C_{Benz.} + \pi C{=}C_{Naphtq.} + nO + nCl + nN \rightarrow \pi C{=}C_{Naphtq.} + nO$	
2	328	328	332	$\pi C{=}C_{Benz.} + nCl + \pi C{=}C_{Naphtq.} \rightarrow \pi C{=}C_{Naphtq.} + nO$	$\pi C{=}C_{Naphtq.} \rightarrow \pi C{=}C_{Naphtq.} + nO$
3	276	280	280	$\pi C{=}C_{Benz.} + \pi C{=}C_{Naphtq.} + nO + nCl + nN \rightarrow \pi^{*}C{=}C_{Naphtq.}$	$\pi C{=}C_{Naphtq.} + nO \rightarrow \pi C{=}C_{Naphtq.} + nO$
4	237	231		$\pi C{=}C_{Naphtq.} \rightarrow \pi^{*}C{=}C_{Naphtq.}$	$\pi C{=}C_{Naphtq.} + nO \rightarrow \pi^{*}C{=}C_{Naphtq.}$
5	139[a]			$\pi C{=}C_{Naphtq.} \rightarrow \pi^{*}C{=}C_{Benz.}$	$nCl + \pi C{=}C_{Naphtq} + \pi C{=}O \rightarrow \pi C{=}C_{Naphtq.} + nO$
				1c	
1	487	490	504	$\pi C{=}C_{Benz.} + \pi C{=}C_{Naphtq.} + nO + nCl + nN \rightarrow \pi C{=}C_{Naphtq.} + nO + nN$	
2	331	335	337	$\pi C{=}C_{Naphtq.} \rightarrow \pi C{=}C_{Naphtq.} + nO + nN$	$\pi C{=}C_{Benz.} + nO + nCl + nN \rightarrow \pi C{=}C_{Naphtq.} + nO + nN$
3	277	279	281	$\pi C{=}C_{Benz.} + \pi C{=}C_{Naphtq.} + nO + nCl + nN \rightarrow \pi^{*}C{=}C_{Naphtq.}$	$C{=}C_{Naphtq.} + nO \rightarrow \pi C{=}C_{Naphtq.} + nO + nN$
4	233	232		$\pi C{=}C_{Naphtq.} \rightarrow \pi^{*}C{=}C_{Naphtq.}$	$nCl + \pi C\text{-}N_{Naphtq.} + \sigma C\text{-}C_{Benz.} + \sigma C\text{-}O_{Benz.} \rightarrow \pi C{=}C_{Naphtq.} + nO + nN$
5	169[a]			$\pi C{=}C_{Benz.} \rightarrow \pi^{*}C{=}C_{Benz.}$	
				1d	
1	493	496	496	$\pi C{=}C_{Benz.} + \pi C{=}C_{Naphtq.} + nO + nCl + nN \rightarrow \pi C{=}C_{Naphtq.} + nO$	
2	332	335	335	$\pi C{=}C_{Naphtq.} \rightarrow \pi C{=}C_{Naphtq.} + nO$	$\pi C{=}C_{Benz.} + nO + nCl \rightarrow \pi C{=}C_{Naphtq.} + nO$
3	280	283	283	$\pi C{=}C_{Benz.} + \pi C{=}C_{Naphtq.} + nO + nCl + nN \rightarrow \pi^{*}C{=}C_{Naphtq.}$	$\pi C{=}C_{Naphtq.} \rightarrow \pi C{=}C_{Naphtq.} + nO$
4	240	230		$\pi C{=}C_{Benz.} + nO + nCl \rightarrow \pi^{*}C{=}C_{Naphtq.}$	$\pi C{=}C_{Benz.} + \pi C{=}C_{Naphtq.} + nO + nCl + nN \rightarrow \pi^{*}C{=}C_{Benz.}$
5	197[a]			$\pi C{=}C_{Naphtq.} \rightarrow \pi^{*}C{=}C_{Naphtq.} + \pi^{*}C{=}C_{Benz.}$	

[a]Estimated spectrum devolution value. n: isolated pair.

information is relevant, since it can provide subsidies for the planning of new 1,4-naphthoquinone derivatives that can be explored for the development of compounds with potentiated biological activities.

Supplementary Information

Crystallographic data (excluding structure factors) for the structures in this work were deposited in the Cambridge Crystallographic Data Centre as supplementary publication number CCDC 2169169. Copies of the data can be obtained, free of charge, via https://www.ccdc.cam.ac.uk/structures/.

Supplementary data are available free of charge at http://jbcs.sbq.org.br as PDF file.

Acknowledgments

The authors acknowledge the financial support received from the Fundação Carlos Chagas de Amparo à Pesquisa do Estado do Rio de Janeiro-FAPERJ (project numbers E-26/210.302/2019 and E-26/211.091/2019), Proppi-UFF (FOPESQ-2020), Conselho Nacional de Desenvolvimento Científico e Tecnológico - Brasil (CNPq) and Coordenação de Aperfeiçoamento de Pessoal de Nível Superior - Brasil (CAPES) for the master and doctorate fellowship granted to R. S. M. Moraes. We thank the PhD Henrique de Castro Silva Junior for the discussion on NBO calculations. We would also like to thank in special the LDRX-UFF, LAME-UFF and LMQC laboratory at Universidade Federal Fluminense.

Author Contributions

Flaviana R. F. Dias was responsible for conceptualization, data curation, formal analysis, investigation, methodology, supervision, validation, writing original draft, review and editing; Vinícius R. Campos for conceptualization, data curation, formal analysis, investigation, methodology, writing original draft, review and editing; Raphael S. M. de Moraes for data curation, formal analysis,

investigation, methodology, validation, visualization, writing original draft, review and editing; Nelson A. Souza for conceptualization, formal analysis, investigation, methodology, validation, writing review and editing; Anna C. Cunha for conceptualization, data curation, formal analysis, investigation, project administration, supervision, writing original draft, review and editing; Mateus R. Lage for Data curation, formal analysis, investigation, methodology, validation, writing original draft, review and editing; Glaucio B. Ferreira for conceptualization, data curation, formal analysis, funding acquisition, investigation, methodology, project administration, supervision, validation, writing original draft.

References

1. Kurban, S.; Deniz, N. G.; Sayil, C.; Ozyurek, M.; Guclu, K.; Stasevych, M.; Zvarych, V.; Komarovska-Porokhnyavet, O.; Novikov, V.; *Heteroat. Chem.* **2019**, *2019*, ID 1658417. [Crossref]
2. Satheshkumar, A.; Ganesh, K.; Elango, K. P.; *New J. Chem.* **2014**, *38*, 993. [Crossref]
3. Campos, V. R.; Cunha, A. C.; Silva, W. A.; Ferreira, V. F.; Santos de Sousa, C.; Fernandes, P. D.; Moreira, V. N.; da Rocha, D. R.; Dias, F. R. F.; Montenegro, R. C.; de Souza, M. C. B. V.; Boechat, F. C. S.; Franco, C. F. J.; Resende, J. A. L. C.; *RSC Adv.* **2015**, *5*, 96222. [Crossref]
4. Novais, J. S.; Campos, V. R.; Silva, A. C. J. A.; de Souza, M. C. B. V.; Ferreira, V. F.; Keller, V. G. L.; Ferreira, M. O.; Dias, F. R. F.; Vitorino, M. I.; Sathler, P. C.; Santana, M. V.; Resende, J. A. L. C.; Castro, H. C.; Cunha, A. C.; *RSC Adv.* **2017**, *7*, 18311. [Crossref]
5. Dias, F. R. F.; Novais, J. S.; Devillart, T. A. N. S.; da Silva, W. A.; Ferreira, M. O.; Loureiro, R. S.; Campos, V. R.; Ferreira, V. F.; de Souza, M. C. B. V.; Castro, H. C.; Cunha, A. C.; *Eur. J. Med. Chem.* **2018**, *156*, 1. [Crossref]
6. Mello, A. L. N.; Sagrillo, F. S.; de Souza, A. G.; Costa, A. R. P.; Campos, V. R.; Cunha, A. C.; Filho, R. I.; Boechat, F. C. S.; Sola-Penna, M.; de Souza, M. C. B. V.; Zancan, P.; *Life Sci.* **2021**, *276*, 119470. [Crossref]
7. Causmaecker, S.; Douglass, J. S.; Fantuzzi, A.; Nitschke, W.; Rutherford, A.W.; *PNAS* **2019**, *116*, 19458. [Crossref]
8. Gutiérrez-Fernández, J.; Kaszuba, K.; Minhas, G. S.; Baradaran, R.; Tambalo, M.; Gallagher, D. T.; Sazanov, L. A.; *Nat. Commun.* **2020**, *11*, 4135. [Crossref]
9. Hui, Y.; Khim Chng, E.; Lin Chng, C. Y.; Poh, H. L.; Webster, R. D.; *J. Am. Chem. Soc.* **2009**, *131*, 1523. [Crossref]
10. Escolastico, C.; Santa Maria, M. D.; Claramunt, R. M.; Jimeno, M. L.; Alkorta, I.; Foces, C.; Cano, F. H.; Elguero, J.; *Tetrahedron* **1994**, *50*, 12489. [Crossref]
11. Catalan, J.; Febero, F.; Guijiarro, M. S.; Claramunt, R. M.; Santa Maria, M. D.; Foces-Foces, M.; Cano, F. H.; Elguero, J.; Sastre, R.; *J. Am. Chem. Soc.* **1990**, *112*, 747. [Crossref]
12. Madhupriya, S.; Elango, K. P.; *Spectrochim. Acta, Part A* **2012**, *97*, 100. [Crossref]
13. Hurvitz, S. A. McAndrew, N. P.; Bardia, A.; Press, M. F.; Pegram, M.; Crown, J. P.; Fasching, P. A.; Ejlertsen, B.; Yang, E. H.; Glaspy, J. A.; Slamon, D. J.; *npj Breast Cancer* **2021**, *7*, 134. [Crossref]
14. Franco, C. F. J.; Jordão, A. K.; Ferreira, V. F.; Pinto, A. C.; de Souza, M. C. B. V.; Resende, J. A. L. C.; Cunha, A. C.; *J. Braz. Chem. Soc.* **2011**, *22*, 187. [Crossref]
15. Dias, F. R. F.; Guerra, F. S.; Lima, F. A.; de Castro, Y. K. C.; Ferreira, V. F.; Campos, V. R.; Fernandes, P. D.; Cunha, A. C.; *J. Braz. Chem. Soc.* **2021**, *32*, 476. [Crossref]
16. Balansa, W.; Mettal, U.; Wuisan, Z. G.; Plubrukarn, A.; Ijong, F. G.; Liu, Y.; Schäberle, T. F.; *Mar. Drugs* **2019**, *17*, 158. [Crossref]
17. Mataracı-Kara, E.; Bayrak, N.; Yıldırım, H.; Yıldız, M.; Ataman, M.; Ozbek-Celik, B.; Tuyun, A. F.; *Med. Chem. Res.* **2021**, *30*, 1728. [Crossref]
18. Neves, A. P.; Barbosa, C. C.; Greco, S. J.; Vargas, M. D.; Visentin, L. C.; Pinheiro, C. B.; Mangrich, A. S.; Barbosa, J. P.; da Costa, G. L.; *J. Braz. Chem. Soc*. **2009**, *20*, 712. [Crossref]
19. da Silva, W. A.; da Silva, L. C.; Campos, V. R.; de Souza, M. C.; Ferreira, V. F.; dos Santos, A. C.; Sathler, P. C.; de Almeida, G. S.; Dias, F. R.; Cabral, L. M.; de Azeredo, R. B.; Cunha, A. C.; *Future Med. Chem.* **2018**, *10*, 527. [Crossref]
20. Saxena, S.; Panchagnula, S.; Sanz, M. E.; Pérez, C.; Evangelisti, L.; Pate, B. H.; *ChemPhysChem* **2020**, *21*, 2579. [Crossref]
21. da Silva, M. N.; Ferreira, V. F.; de Souza, M. C. B. V.; *Quim. Nova* **2003**, *26*, 407. [Crossref]
22. Xiong, Y.; Kaw, H. Y.; Zhu, L.; Wang, W.; *Crit. Rev. Environ. Sci. Technol.* **2021**. [Crossref] accessed in April 2022
23. Francisco, A. I.; Casellato, A.; Neves, A. P.; Carneiro, J. W. M.; Vargas, M. D.; Visentin, L. C.; Magalhães, A.; Câmara, C. A.; Pessoa, C.; Costa-Lotufo, L. V.; Marinho Filho, J. D. B.; de Moraes, M. O.; *J. Braz. Chem. Soc.* **2010**, *21*, 169. [Crossref]
24. da Silva Jr., E. N.; de Souza, M. C.; Fernandes, M. C.; Menna-Barreto, R. F.; Pinto, M. C. F. R.; Lopes, F. A.; de Simone, C. A.; Andrade, C. K. Z.; Pinto, A. V.; Ferreira, V. F.; de Castro, S. L.; *Bioorg. Med. Chem.* **2008**, *16*, 5030. [Crossref]
25. da Silva Jr., E. N.; Menna-Barreto, R. F.; Pinto, M. C. F. R.; Silva, R. S. F.; Teixeira, D. V.; de Souza, M. C. B. V.; de Simone, C. A.; de Castro, S. L.; Ferreira, V. F.; Pinto, A. V.; *Eur. J. Med. Chem.* **2008**, *43*, 1774. [Crossref]
26. Schepetkin, I. A.; Karpenko, A. S.; Khlebnikov, A. I.; Shibinska, M. O.; Levandovskiy, I. A.; Kirpotina, L. N.; Danilenko, N. V.; Quinn, M. T.; *Eur. J. Med. Chem.* **2019**, *183*, 111719. [Crossref]
27. dos Santos, E. V.; Carneiro, J. W. M.; Ferreira, V. F.; *Bioorg. Med. Chem.* **2004**, *12*, 87. [Crossref]
28. Pereira-da-Silva, J.; Mendes, M.; Kossoski, F.; Lozano, A. I.; Rodrigues, R.; Jones, N. C.; Hoffmann, S. V.; Ferreira da Silva, F.; *Phys. Chem. Chem. Phys.* **2021**, *23*, 2141. [Crossref]

29. Tandon, V. K.; Maurya, H. K.; *Tetrahedron Lett.* **2009**, *50*, 5896. [Crossref]
30. Prado, L. D.; Santos, A. B. X.; Rocha, H. V. A.; Ferreira, G. B.; Resende, J. A. L. C.; *Int. J. Pharm.* **2018**, *553*, 261. [Crossref]
31. Marques, M. M.; Rezende, C. A.; Lima, G. C.; Marques, A. C. S.; Prado, L. D.; Leal, K. Z.; Rocha, H. V. A.; Ferreira, G. B.; Resende, J. A. L. C.; *J. Mol. Struct.* **2017**, *1137*, 476. [Crossref]
32. *APEX3*, version 2015.5-2; Bruker AXS Inc., Madison, Wisconsin, USA, 2015.
33. *SAINT*, version 8.34A; Bruker AXS Inc., Madison, Wisconsin, USA, 2013.
34. *SADABS*, v2014/5; Bruker AXS Inc., Madison, Wisconsin, USA, 2014.
35. Sheldrick, G. M.; *Acta Crystallogr., Sect. C: Struct. Chem.* **2015**, *71*, 3. [Crossref]
36. Sheldrick, G. M.; *Acta Crystallogr., Sect. A: Found. Adv.* **2015**, *71*, 3. [Crossref]
37. Macrae, C. F.; Edgington, P. R.; McCabe, P.; Pidcock, E.; Shields, G. P.; Taylor, R.; Towler, M.; van de Streek, J.; *J. Appl. Crystallogr.* **2006**, *39*, 453. [Crossref]
38. Dolomanov, O. V.; Bourhis, L. J.; Gildea, R. J.; Howard, J. A. K.; Puschmann, H.; *J. Appl. Crystallogr.* **2009**, *42*, 339. [Crossref]
39. Frisch, M. J. E. A.; Trucks, G. W.; Schlegel, H. B.; Scuseria, G. E.; Robb, M. A.; Cheeseman, J. R.; Scalmani, G.; Barone, V.; Mennucci, B.; Petersson, G. A.; Nakatsuji, H.; Caricato, M.; Li, X.; Hratchian, H. P.; Izmaylov, A. F.; Bloino, J.; Zheng, G.; Sonnenberg, J. L.; Hada, M.; Ehara, M.; Toyota, K.; Fukuda, R.; Hasegawa, J.; Ishida, M.; Nakajima, T.; Honda, Y.; Kitao, O.; Nakai, H.; Vreven, T.; Montgomery Jr., J. A.; Peralta, J. E.; Ogliaro, F.; Bearpark, M.; Heyd, J. J.; Brothers, E.; Kudin, K. N.; Staroverov, V. N.; Kobayashi, R.; Normand, J.; Raghavachari, K.; Rendell, A.; Burant, J. C.; Iyengar, S. S.; Tomasi, J.; Cossi, M.; Rega, N.; Millam, J. M.; Klene, M.; Knox, J. E.; Cross, J. B.; Bakken, V.; Adamo, C.; Jaramillo, J.; Gomperts, R.; Stratmann, R. E.; Yazyev, O.; Austin, A. J.; Cammi, R.; Pomelli, C.; Ochterski, J. W.; Martin, R. L.; Morokuma, K.; Zakrzewski, V. G.; Voth, G. A.; Salvador, P. S.; Dannenberg, J. J.; Dapprich, S.; Daniels, A. D.; Farkas, O.; Foresman, J. B.; Ortiz, J. V.; Cioslowski, J.; Fox, D. J.; *Gaussian 09*, version G09 D, Gaussian Inc, Wallingford, Connecticut, 2009.
40. Yanai, T.; Tew, D. P.; Handy, N. C.; *Chem. Phys. Lett.* **2004**, *393*, 51. [Crossref]
41. Komjáti, B.; Urai, Á.; Hosztafi, S.; Kökösi, J.; Kováts, B.; Nagy, J.; Horváth, P.; *Spectrochim. Acta, Part A* **2016**, *155*, 95. [Crossref]
42. Tomasi, J.; Mennucci, B.; Cammi, R.; *Chem. Rev.* **2005**, *105*, 2999. [Crossref]
43. Francl, M. M.; Pietro, W. J.; Hehre, W. J.; *J. Chem. Phys.* **1982**, *77*, 3654. [Crossref]
44. Singh, U. C.; Kollman, P. A.; *J. Comput. Chem.* **1984**, *5*, 129. [Crossref]
45. Besler, B. H.; Merz Jr., K. M.; Kollman, P. A.; *J. Comput. Chem.* **1990**, *11*, 431. [Crossref]
46. O'boyle, N. M.; Tenderholt, A. L.; Langner, K. M.; *J. Comput. Chem.* **2008**, *29*, 839. [Crossref]
47. Zhurko, G. A.; *Chemcraft - Graphical Software for Visualization of Quantum Chemistry Computations*, version 1.8 (build 622b); Ivanovo, Russia, 2005.
48. Jamróz, M. H.; *Spectrochim. Acta, Part A* **2013**, *114*, 220. [Crossref]
49. Glendening, E. D.; Landis, C. R.; Weinhold, F.; *WIREs Comput. Mol. Sci.* **2012**, *2*, 1. [Crossref]
50. Weinhold, F.; *J. Comput. Chem.* **2012**, *33*, 2363. [Crossref]
51. Glendening, E. D.; Weinhold, F.; *J. Comput. Chem.* **1998**, *19*, 593. [Crossref]
52. Glendening, E. D.; Weinhold, F.; *J. Comput. Chem.* **1998**, *19*, 610. [Crossref]
53. Glendening, E. D.; Badenhoop, J. K.; Weinhold, F.; *J. Comput. Chem.* **1998**, *19*, 628. [Crossref]
54. Rajalakshmi, P.; Jayasudha, P.; Ciattini, S.; Chelazzi, L.; Elango, K. P.; *J. Mol. Struct.* **2019**, *1195*, 259. [Crossref]
55. Win, T.; Yerushalmi, S.; Bittner, S.; *Synthesis* **2005**, *10*, 1631. [Crossref]
56. Bayrak, N.; Yıldız, M.; Yıldırım, H.; Sahin, M.; Tuyun, A. F.; *Bull. Chem. Soc. Ethiop.* **2018**, *32*, 603. [Crossref]
57. Jeyavijayan, S.; Palanimurugan; Viswanathan, K.; Lavanya, V.; Gurushankar, K.; *Rasayan J. Chem.* **2019**, *12*, 21. [Crossref]
58. Kulkarni, S. V.; Sarawadekar, R. G.; Pawar, A. B.; *Int. J. ChemTech Res.* **2017**, *10*, 239. [Link] accessed in April 2022
59. Ali, N.; Mansha, A.; Asim, S.; Ali, H. S.; Usman, M.; *J. Struct. Chem.* **2020**, *61*, 182. [Crossref]
60. Delarmelina, M.; Ferreira, G. B.; Ferreira, V. F.; Carneiro, J. W. M.; *Vib. Spectrosc.* **2016**, *86*, 311. [Crossref]
61. Zanoni, M. V. B.; Yanamaka, H.; *Corantes: Caracterização Química, Toxicológica, Métodos de Detecção e Tratamento*, vol. 1, 1st ed.; Cultura Acadêmica: São Paulo, Brazil, 2016.
62. Souza, N. A.; Borges, M. N.; Ribeiro, C. M. R.; Trales, P. R.; *Rev. Iberoam. Educ.* **2008**, *46*, 1. [Crossref]
63. Martins, G. B. C.; Sucupira, R. R.; Suarez, P. A. Z.; *Rev. Virtual Quim.* **2015**, *7*, 1508. [Crossref]
64. Trommsdorff, H. P.; *J. Chem. Phys.* **1972**, *56*, 5358. [Crossref]
65. Borges, R. S.; Carneiro, A. S.; Barros, T. G.; Barros, C. A. L.; Chaves Neto, A. M. J.; da Silva, A. B. F.; *J. Mol. Model.* **2014**, *20*, 2541. [Crossref]
66. Monks, T. J.; Jones, D. C.; *Curr. Drug Metab.* **2002**, *3*, 425. [Crossref]

Submitted: April 30, 2022
Published online: July 28, 2022

This is an open-access article distributed under the terms of the Creative Commons Attribution License.